ISAS - INTERNATIONAL SCHOOL FOR ADVANCED STUDIES

Thesis submitted for the degree of
"Doctor Philosophiae"

Quantum Molecular Dynamics Study of Dilute Na-NaBr Liquid Solutions

CANDIDATE
XU Lifang

SUPERVISORS
Prof. A. Selloni
Prof. M. Parrinello

Academic Year 1988/89

TRIESTE

SISSA - SCUOLA INTERNAZIONALE SUPERIORE DI STUDI AVANZATI
TRIESTE
Strada Costiera 11

Scuola Internazionale Superiore di Studi Avanzati

International School for Advanced Studies

Quantum Molecular Dynamics Study of Dilute Na-NaBr Liquid Solutions

Thesis submitted for the degree of

"Doctor Philosophiæ"

CANDIDATE

XU Lifang

SUPERVISORS

Prof. A. Selloni

Prof. M. Parrinello

October 1989

ACKNOWLEDGEMENTS

I would like to express my gratitude to Professor Annabella Selloni for her patient instructions, kind guidance and careful checks during the course of this work, as well as reading of the manuscript. I would like to express my cordial thanks to Professor Michele Parrinello for his ideas and kind guidance. I am grateful to Dr. E. Fois for his help in computer programs at the early stage of this work.

This work has been in part supported by the SISSA-CINECA (Centro di Calcolo Elettronico dell'Italia Nord-Orientale) collaborative project, under the sponsorship of the Italian Ministry for Public Education.

Contents

Chapter 1

Introduction

In this first chapter we briefly review the general phenomenology of metal-molten salt solutions and the peculiar behavior of Na-NaX solutions.

1.1 A short review on metal-molten salt solutions

Solutions of alkali metals in their liquid halides (M-MX) display an intriguing variety of behavior as a function of temperature and concentration [1,2]. They exhibit a range of liquid-liquid immiscibility below a critical temperature T_c. At elevated temperature above T_c, a transformation from non-metallic (NM) to metallic (M) states can be continuously studied in a homogeneous liquid phase. The critical metal mole fractions x near the consolute temperature typically range from $0.2 \leq x \leq 0.6$ in the different M-MX solutions.

Despite the long history of research on metal-metal halide melts,

vigorous activity has continued to grow up to the present. Much of the most recent work has been motivated by strong interest in the electronic states and metal-nonmetal transition. In the last few years not only further studies of basic physical properties such as electronic conductivity, density and magnetic susceptibility, but also increasing use of spectroscopic techniques such as optical absorption, nuclear magnetic resonance, electron spin resonance and neutron scattering, as well as computer simulation techniques. These new approaches have resulted in the resolution of some long-standing problems concerning the electronic properties of the solutions and have uncovered new features of the transition of a metal into a nonmetallic ionic state.

The structure of pure molten salts is closely related to the degree of dissociation. Alkali halide melts are fully dissociated ionic liquids in which the inter-ionic coulomb forces impose a large measure of compositional order. This means that a metal cation M^+ has a high probability of being surrounded by a number (4-6) of halide anions X^- and vice versa. Many polyvalent metal halides, in contrast, retain substantial molecular character in the melt. Whatever the structure of the pure molten salt, the central question raised by solution of small quantities of metal concerns the state of the 'excess' electrons – the valence electrons of the dissolved metal. There are many possible states that may be formed: retention of the electrons by the ions to form dissolved neutral atoms; delocalized dilute metallic states; Mott-Anderson multi-site localized states; polaronic states (F-center); metal dimers and small metal clusters. Determination of the electronic state and transport mechanism for low metal concentrations in molten halides is not only basic for un-

derstanding the physics inside, but also crucial for understanding the subsequent transition to the metallic state at higher concentrations. We shall see, after comparing Na-NaBr with K-KCl solutions, that there is no universal description of the excess electron and different possibilities mentioned above maybe occur in different solutions.

In this thesis we shall restrict our attention to extremely small concentration of excess metal ($x \sim 3.1\%$ and $\sim 6.2\%$). At present the general consensus in this dilute limit is that the added metal atom dissociates into M^+ and e^- and forms a localized state analogous to F-centers in ionic solids. The physical picture underlying the model is that the e^- substitutionally occupies the place of an X^-. This F-center model describes quite well several sets of experimental data in various M-MX system and is confirmed by recently developed computer simulation techniques.

Freyland *et al.* [3,4] investigated the optical properties of liquid alkali metal-alkali halide solutions for different metal concentrations and temperatures. If one adds a small amount ($x \sim 0.01$) of alkali metal to one of its molten halides, the otherwise colourless melt becomes strongly coloured. This effect is due to a strong absorption band in the visible or near infrared. These bands are remarkably similar to those associated with F-centers in additively coloured alkali halide crystals, although the liquid-state spectra are typically shifted to the red by a few tenths of an electron-volt. Absorption bands essentially identical to those in liquid alkali metal-halide solutions were also obtained by Schmitt & Schindewolf [5] using direct injection of electrons into pure alkali halides.

Pitzer [6] proposed that excess electrons in liquid alkali halides form

F-center analogues. The optical absorption would be due to electronic transitions to the first excited state. These may differ from those in the crystal in the cavity size, number of coordinating metal ions, lack of well defined symmetry, *etc.*

Nicoloso & Freyland [7] obtained that the electrons contribute Curie-type paramagnetism. This indicates that excess electrons are localized in the dilute limit. Warren *et al.* [8] studied nuclear magnetic relaxation of Cs-CsI and showed that the localization times are comparable with the diffusion-limited lifetime of a local configuration of ions.

One indication of the structure of the localized states is provided by the magnitudes of the hyperfine fields. Warren *et al.* [8] found that the fields are too low to be explained by atomic or multi-site localized states. The hyperfine field is a measure of the charge on the sites of the resonant nuclei, so these results indicate that the charge is distributed mainly off the size as should be the case for the F-center. Electron spin resonance has been observed for low metal concentrations in various alkali halide eutectic mixture by Nicoloso & Freyland[9]. The measured shifts of the electronic g-factor are consistent with the F-center model.

Parrinello & Rahman [10] have shown how the dilute metal-salt solutions can be modelled using a combination of molecular dynamics and Feynman path integral techniques. In this approach the quantum problem is shown to be isomorphic to an appropriate classical problem. The solvated electron is mapped on a closed flexible polymer of P points. In their calculation the electron tends to form a compact highly localized charge distribution. Their result for the electron-cation correlation function $g_{e,+}(r)$ shows the F-center character of the electronic state by

the peak in $g_{e,+}(r)$ at finite $r_0 \sim 2(\mathring{A})$. The coordination number for the electron is approximately 4 metal ions.

Selloni *et al.* [11] have adopted a mixed quantum-classical approach to study electronic states and dynamical properties of dilute liquid K-KCl, in which electrons are dealt with quantum mechanically, while ions classically. This method will be reviewed below in Chapter 2. In their calculations excess electrons spend most of their time in localized F-center states. The calculation confirmed the F-center model and clarified the nature of the electronic states and dynamical properties.

1.2 The peculiar behavior of Na-NaBr solutions

Some properties of liquid Na solutions are known to differ significantly from those of solutions involving heavier alkali metals. Much attention has been focused in particular on the so called "conductivity dilemma"[12]. Addition of only a few mole % of alkali metal to a molten halide introduces an electronic contribution to the electronic conductivity. Na solutions have a striking different property compared with the heavier alkali metals K, Rb and Cs. Whereas the conductivity of the latter systems increases rapidly, roughly exponentially with x, the increase in Na solution is sublinear at temperature $T < T_c$. At much higher temperatures, the conductivity variation becomes comparable with those of the other metal solutions.

In the early work of Bronstein & Bredig [12] it was suggested that formation of Na_2 dimers at low temperature might effectively reduce the

concentration of conducting electrons and thus lower the conductivity at higher metal concentrations. Later, Katz & Rice [13] and Durham & Greenwood [14] offered alternative explanations based on reduced electronic mobilities at higher metal concentrations. More recently the formation of Na^- species has been also suggested [15].

A comparison of nuclear magnetic resonant properties of Na-NaBr,

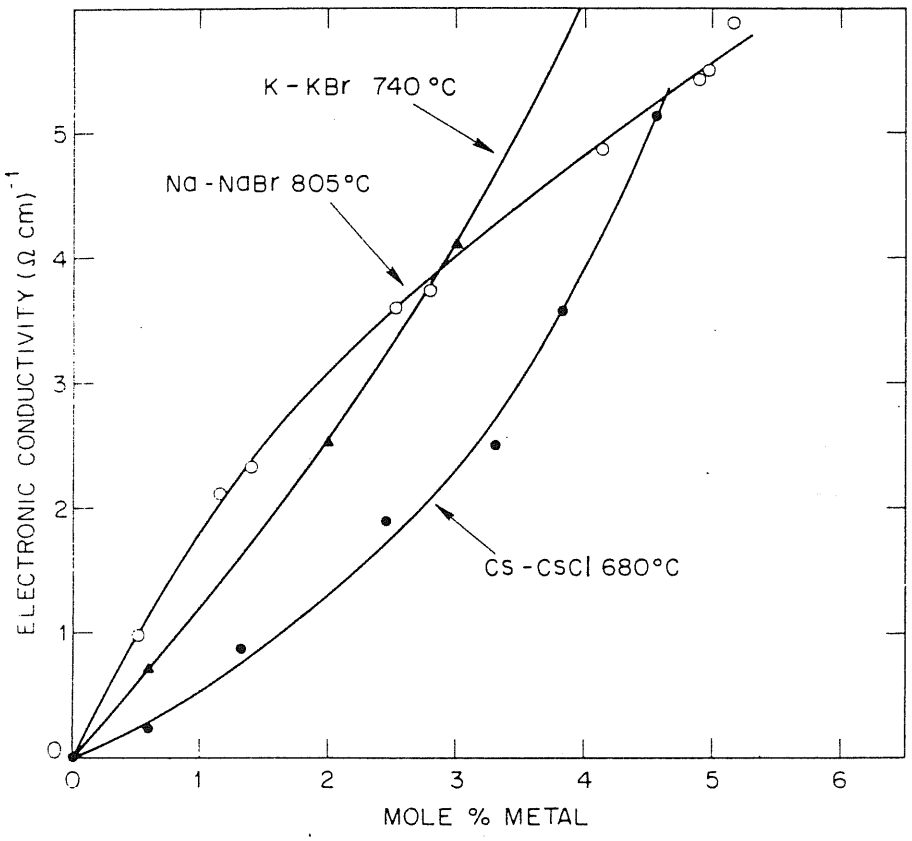

Figure 1.1: Electronic conductivity versus excess metal content in dilute alkali metal-alkali halide melts. Negative curvature is typical of Na-NaX solutions at temperatures well below T_c[1].

Cs-CsCl and Cs-CsI by Warren *et al.* [16] separates the effects of electron concentration and the mobility and supports the original ideas of Bronstein and Bredig. The electron concentration in Na-NaBr is reduced at high metal concentration by formation of states which are both non-magnetic and non-conducting. The dimer Na_2 and/or the Na^- ion would satisfy this criterion.

The following picture of transport at low metal concentrations has emerged from the foregoing experiments. In Na solutions at low temperature, a certain fraction of excess electrons is removed from the conductivity process by formation of species such as Na_2 and/or Na^-. These are stable for times long compared with the jump times of the remaining electrons. The mobility of the remainder is determined by the lifetime of a favourable site for localization and is independent of concentration. When such a site is disrupted by ionic diffusion, the electron enters an extended state at the conduction band edge [17] and moves rapidly a distance to a new localization site. Warren *et al.*[16] found the mean-square jump distance $< a^2 >^{1/2} \sim 20\mathring{A}$ from the correlation time and conductivity values. A similar distance is found for the Cs solutions, but the mobility is strongly dependent on concentration. A possibility suggested by the authors is that species such as Cs_2 also tend to form in the caesium solutions, but they are in rapid equilibrium with localized states so that their lifetime are less than or comparable with the solvation time. The mobility would be enhanced by this equilibrium since an electron can be localized at a new site after formation and dissociation of the species.

Another example of the special behavior of Na-NaX systems is pro-

vided by the optical absorption spectrum, which is usually considered as the strongest evidence in favor of the F-center model. In the crystalline state, Mollwo and Ivey reported an empirical relation between the maximum energy of the F-band, ϵ_m, and the interionic separations, $r_+ + r_-$, which reveals the main optical characteristic of the F-center, the so-called Mollwo-Ivey relation (see, e.g., Ref.[18,19]). The investigations of the optical absorption constant by Freyland *et al.* [4] show that the peak energy of Na-NaBr does not satisfy the Mollwo-Ivey relation,

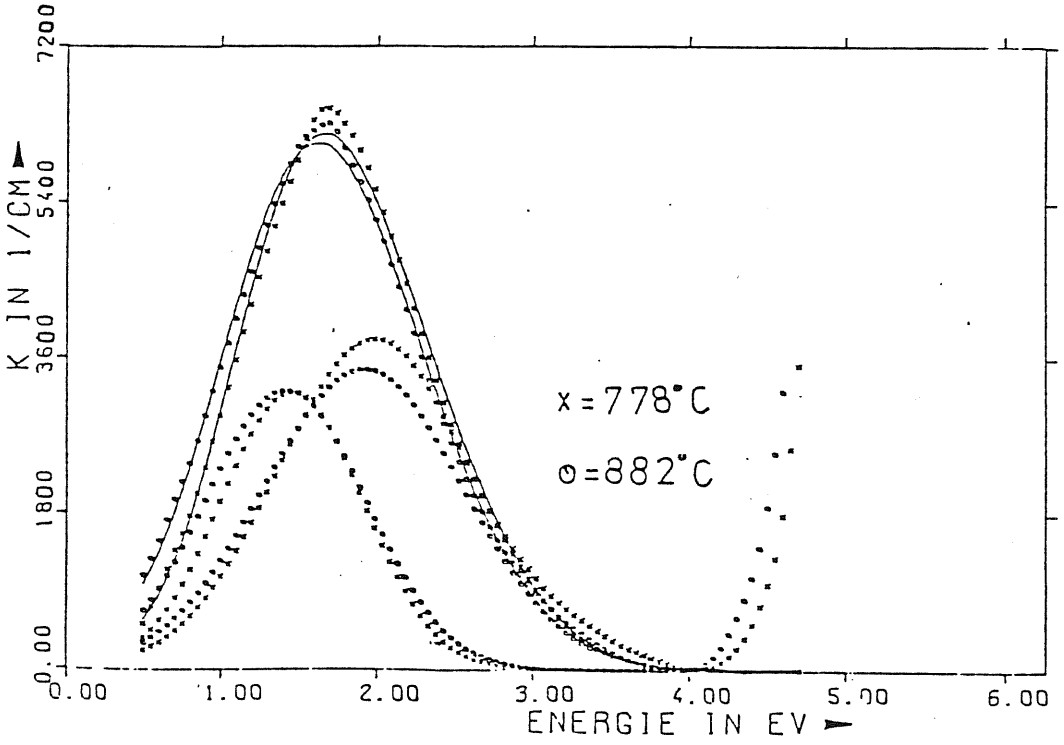

Figure 1.2: Optical absorption constant versus photon energy of liquid Na-NaBr solutions at metal concentration $x = 4.2\%$ for different temperatures[4].

while in the other solutions, the relation is satisfied:

$$\epsilon_m = 13.0(r_+ + r_-)^{-2.03} \tag{1.1}$$

Here ϵ_m is in electronvolts at a constant reduced temperature of $T/T_m = 1.08$ with T_m the melting point of salts, and interionic distance in angstroms. The spectrum of Na-NaBr is particular broad and the absorption band at 1.65 eV occurs which can be deconvoluted into two bands, one at 1.42 eV that the authors interpreted as the F-band, due to that this energy satisfies the relation (1.1), and an additional band at 1.8 eV (see Figure 1.2). The origin of this behavior is not clear.

1.3 Plan and goal of the thesis

In this thesis we have studied the electronic states and dynamical properties of dilute liquid Na-NaX solutions by using a recently developed Quantum Molecular Dynamics (QMD) method[11,20]. The aim of our research is to understand the peculiar behavior of Na-NaX solutions described above. We performed calculations for one ($x \sim 0.031$) and two ($x \sim 0.061$) excess electrons in molten NaBr. In the single electron case we found that the excess electron forms a dipolar Na atomic-like state that is rather different from the F-center-like states formed in the solutions involving heavier alkali metals. Several features of the peculiar behavior of Na-NaBr solution can be related to formation of this dipolar atomic states, which is similar to that proposed by Logan [21,22,23] and offers a simple clue to understand the optical spectrum. At higher concentration spin pairing occurs and various species are observed. The most likely complexes are found to be Na^- and Na_2, in agreement with

earlier speculations [12,16] and at variance with that found in K-KCl [20,24]. We also show that the greater strength of the $Na^+ - e$ potential in mostly responsible for the different behavior of the electronic states in Na-NaBr.

This thesis is organised as follows. In chapter 2 the QMD method is reviewed both for one and two excess electrons. In chapter 3 we present our model calculations for NaBr solutions. Here some technical aspects are also described. In Chapter 4 we describe the structure of electron states in Na-NaBr solutions by calculating the electron-ion correlation functions and studying the time evolution of the relative distance between the center of mass of the electron and ions closest to it. The results for K-KCl solution are also shown for comparison. In chapter 5 the dynamical properties, and in particular the optical spectra are discussed. Finally, in chapter 6 we present our conclusions.

Chapter 2

The QMD Method

Recently developed computer simulation methods such as the Path Integral (PI) [10], the Car-Parrinello [25] and the Quantum Molecular Dynamics (QMD) methods [11,20] provide very powerful tools to study the static and dynamical properties of a variety of materials.

In this chapter first we give a brief description of the classical Molecular Dynamics (CMD) method and then the QMD method for a single and two solvated electrons is reviewed. In QMD approach we confine ourselves to the Born-Oppenheimer (BO) approximation. Namely, we assume that the electrons always remain in the ground state pertaining to the instantaneous ionic configuration. In the case of a many electron system, a further approximation is that of treating the electronic quantum many body problem in the Local Spin Density (LSD) approximation. In so doing we will loose information on the full many body wavefunction and focus only on the electron density and spin polarization. The validity of these two approximations will be discussed again below, for the various systems of interest.

2.1 Classical Molecular Dynamics

The molecular dynamics method [26] consists in computing phase space trajectories of a collection of molecules, which individually obey the classical laws of motion, and to perform time average along the computed trajectories. By the ergodic hypothesis, such time averages are then treated as the thermodynamic ensemble averages for equilibrium systems.

The approach taken by the MD method is to solve the equations of motion numerically on a computer. To do so the equations are approximated by suitable schemes, ready for numerical evaluation on a computer. The order of the error depends on the specific approximation, i.e., the resulting algorithm. In principle, the error can be made as small as desired, restricted only by the speed and memory of the computer.

Let the system consist of N particles. For practical reasons, N is chosen to be finite. Since we restrict ourselves to properties of the bulk at a specific density ρ we must introduce a volume, the MD-cell, to retain a constant density. For computational simplicity a cubic volume is usually chosen with volume $V = L^3$. The introduction of the box creates six unwanted surfaces. To reduce the effect of the surfaces periodic boundary conditions, i.e., the basic cell is repeated identically an infinite number of times, is imposed.

From a numerical point of view the MD method is an initial value problem. One can derive recursion relations for the positions and/or velocities (momenta) from the differential equations. These algorithms perform in a step-by-step way. At each step an approximation for the

positions and velocities is obtained, first at time t_1, then at $t_2 > t_1$, *etc.* Hence, the integration proceeds in the time direction (time integration algorithms). The recursion relation must clearly allow efficient evaluation. In addition, the scheme must be numerically stable.

The implementation of the classical MD is straightforward. For a system of N classical particles with the interaction potential $\Phi(\vec{R}_1, \ldots, \vec{R}_N)$, the trajectories, i.e. the coordinates $\vec{R}_I(t)$ and velocities $\dot{\vec{R}}_I(t)$ at time t, $(I = 1, \ldots, N)$, can be obtained through a numerical integration of Newton's equations

$$M_I \ddot{\vec{R}}_I = -\nabla_{\vec{R}_I} \Phi(\vec{R}_1, \ldots, \vec{R}_N), \quad I = 1, \ldots, N \tag{2.1}$$

where the dots indicate time derivatives, and M_I is the mass of the I-th particle. The major input is the interaction potential that governs the motion of particles.

The CMD method is, however, restricted to the treatment of classical particles and cannot give information about quantum effects in the system, which is an important facet of the physics of metal-molten salt solutions. In particular questions such as the electronic states, the nature of electronic diffusion processes and excitation spectra cannot be answered by classical MD method. From this point of view, it is necessary to introduce an approach which deals with the quantum particles, i.e., the excess electrons, by quantum mechanics.

2.2 One electron

We adopt a mixed quantum-classical approach in which the excess electron is described by its wavefunction $\psi(r, t)$ and the ions by their po-

sition $\{R\}$. The time evolution of $\psi(r,t)$ is obtained by solution of the time-dependent Schrödinger equation (TDSE)

$$i\frac{\partial\psi(r,t)}{\partial t} = H_{eI}(\{R\})\psi(r,t) \tag{2.2}$$

with $H_{eI} = T + V_{eI}$, where $T = -1/2\nabla^2$ is the kinetic energy operator and $V_{eI} = V_{eI}(r,\{R\})$ the electron-ion potential. Since V_{eI} depends on the ionic coordinates which vary in time due to the ionic motion, the operator $H(\{R\})$ changes in time. We shall denote by $\phi_n(\{R\})$ and $E_n(\{R\})$ the n-th electronic eigenstate and eigenvalue corresponding to the instantaneous ionic configuration $\{R\}$. The ionic motion is in turn obtained by solving the classical equations

$$M_I\frac{\partial^2 R_I}{\partial t^2} = -\frac{\partial V_{II}(\{R\})}{\partial R_I} - \int dr|\psi(r,t)|^2\frac{\partial V_{eI}(r,\{R\})}{\partial R_I} \tag{2.3}$$

where M_I is the mass of the I-th ion and V_{II} the interionic potential. It is important to realize which are the conditions of validity of the set of Eqs. (2.2) and (2.3). Since these equations assume separability of the electronic and ionic motions, they will be valid only if the motion is adiabatic, *i.e.* if the electron is always in a given eigenstate of the instantaneous Hamitonian [27], e.g. in the ground state $\phi_0(\{R\})$. This requires the electronic excitation energy Δ to be always greater than the ionic kinetic energies ($\sim kT$), for any accessible ionic configuration. Viceversa, if for some $\{R\}$, Δ becomes of the order of or smaller than kT, an electronic transition may take place. In this approach the occurrence of a non-adiabatic event is indicated by the fact that $\psi(r,t)$ does no longer coincide with the ground state $\phi_0(\{R(t)\})$, but becomes a linear combination of various $\phi_n(\{R(t)\})$. In this method it is therefore

important to periodically check the adiabaticity of the motion. This is done by projecting the current electronic state onto the ground state $\phi_0(\{R(t)\})$ of the instantaneous Hamitonian $H(\{R(t)\})$, i.e.

$$P_0(t) \equiv | < \phi_0(\{R(t)\})|\psi(t) > |^2. \tag{2.4}$$

Non-adiabatic events are indicated by a rather sudden change of $P_0(t)$. After such events the scheme becomes invalid.

For our special example of electrons solvated in a molten salt, we found that at equilibrium the energy gap Δ between the ground state and the first excited state is usually much greater than kT. In one of our runs for NaBr we found a small departure from adiabaticity ($P_0 \sim 0.97$) for which no special intervention was used, whereas in another run the electronic motion was always in the ground state ($P_0 \geq 0.99$) in a rather long calculation ($\sim 6 \times 10^5 \Delta t$). This indicates that the behavior of the system is ground state dominated and non-adiabatic events occur with extremely low probability. For the calculation of most physical properties the neglect of these non-adiabatic effects should thus be justified.

The coupled set of Eqs. (2.2) and (2.3) is solved numerically by sequential updating of ψ and $(\{R\})$. The standard Verlet algorithm [28] is used to solve Eq. (2.3)

$$R_I(t + \Delta t) = -R_I(t - \Delta t) + 2R_I(t) + f_I \Delta t^2 + O[(\Delta t)^4] \tag{2.5}$$

where

$$f_I = -\frac{\partial V_{II}(\{R\})}{\partial R_I} - \int dr |\psi(r,t)|^2 \frac{\partial V_{eI}(r,\{R\})}{\partial R_I}.$$

For the TDSE we use instead the product formula

$$\psi(r, t + \Delta t) = e^{-iH(t)\Delta t}\psi(t)$$

$$\sim e^{-iV_{eI}\Delta t/2}e^{-iT\Delta t}e^{-iV_{eI}\Delta t/2}\psi(r,t) + O[(\Delta t)^3]. \qquad (2.6)$$

Successive applications of the operators $e^{-iV_{eI}\Delta t/2}$ and $e^{-iT\Delta t}$ are performed switching from real space (where V_{eI} is diagonal) to reciprocal space (where T is diagonal) and viceversa by Fast Fourier Transform (FFT) techniques[29,30] (A more detailed description of the solution of the TDSE is given in Appendix A). It appears that the approximation formula (2.6) maintains the unitarity of the Schrödinger time evolution, and therefore the norm of the wavefunction ψ.

The time step Δt to be used in the integration procedure (2.6) must be small with respect to the inverse of a typical electronic frequency, e.g. Δ^{-1}. On the other hand, the difference in time scale between the electronic and ionic motions usually allows us to use a larger time step ΔT to integrate the equation (2.5). In our calculations we used $\Delta t \sim \ 1a.u. = 2.4 \times 10^{-17}s$ and $\Delta T = 10 \times \Delta t$. With this choice, conservation of the total energy

$$E_T = < \psi(t)|H(\{R(t)\})|\psi(t) > + \sum_I \frac{1}{2}M_I\dot{R}_I^2 + V_{II}(\{R(t)\}) \qquad (2.7)$$

was rather satisfactory ($|\Delta E_T/E_T| < 10^{-3}$ in a run of $\sim 6 \times 10^5 \Delta t$).

2.3 Two electrons

In this section we will extend the approach described in the previous section to a multielectron system. Due to the great difficulty of dealing with a many-body wavefunction, an exact treatment is impossible in practice. An accurate and practically very convenient solution of the quantum many-body problem can however be obtained by using the

Local Spin Density (LSD) approximation to Spin Density Functional (SDF) theory [31,32]. Using this approach, we describe a N-electron system in terms of N one-particle wavefunctions $\psi_{i\alpha}(r,t)$ (here $\alpha = \uparrow, \downarrow$ is the spin label respect to spin up and down). The $\psi_{i\alpha}(r,t)$ obey the time-dependent Kohn-Sham (KS) equations

$$i\hbar\frac{\partial\psi_{i\alpha}(r,t)}{\partial t} = [-\frac{1}{2}\bigtriangledown^2 + V_{eI}(r,\{R\}) + V_H(r) + V_{xc,\alpha}(r)]\psi_{i\alpha}(r,t) \quad (2.8)$$

subject to the initial conditions

$$\psi_{i\alpha}(t_0) = \phi^0_{i\alpha}(\{R(t_0)\}),$$

where V_H and $V_{xc,\alpha}$ are the Hartree and spin-dependent exchange-correlation potentials respectively, and $\{\phi^0_{i\alpha}(\{R(t_0)\})\}$ is the set of one-particle wavefunctions describing the electronic ground state corresponding to the ionic configuration $\{R(t_0)\}$. The set $\{\phi^0_{i\alpha}(\{R(t_0)\})\}$ is obtained by minimization of the energy functional

$$\begin{aligned} E = -\frac{1}{2}\sum_{i\alpha}\int dr\phi^*_{i\alpha}(r)\nabla^2\phi_{i\alpha}(r) \\ + \int drn(r)V_{eI}(r,\{R\}) \\ +\frac{1}{2}\int dr\int dr'\frac{n(r)n(r')}{|r-r'|} + E_{xc}[n_\uparrow, n_\downarrow] \end{aligned} \quad (2.9)$$

with respect to the $\{\phi_{i\alpha}(r)\}$. Here $E_{xc}[n_\uparrow, n_\downarrow]$ is the exchange-correlation functional. In the LSD approximation

$$E^{LSD}_{xc}[n_\uparrow, n_\downarrow] = \int drn(r)\varepsilon_{xc}(n_\uparrow(r), n_\downarrow(r)) \quad (2.10)$$

where $\varepsilon_{xc}(n_\uparrow, n_\downarrow)$ is the exchange correlation energy per particle of the homogeneous electron gas with spin density $n_\uparrow$ and $n_\downarrow$. The total density $n(r)$ is defined as

$$n(r) = \sum_i |\phi_{i,\uparrow}(r)|^2 + \sum_i |\phi_{i,\downarrow}(r)|^2$$
$$\equiv n_\uparrow(r) + n_\downarrow(r) \tag{2.11}$$

It is customary to discuss ε_{xc} in terms of

$$r_s = \left(\frac{3}{4\pi n}\right)^{1/3} \tag{2.12}$$

for the density, and spin polarization

$$\zeta(r) = \frac{n_\uparrow(r) - n_\downarrow(r)}{n(r)} \tag{2.13}$$

The Monte Carlo results of Ceperley and Alder [33], parametrized by Perdew and Zunger [34], are used for the calculations of ε_{xc} for both the unpolarized (U, $\zeta = 0$) and polarized (P, $\zeta = 1$) cases. For intermediate spin polarizations $0 < \zeta < 1$, we used a standard interpolation formula, in which the correlation energy has the same polarization dependence as the exchange energy

$$\varepsilon_{xc}(r_s, \zeta) = \varepsilon_{xc}^U(r_s) + f(\zeta)[\varepsilon_{xc}^P(r_s) - \varepsilon_{xc}^U(r_s)] \tag{2.14}$$

where

$$f(\zeta) = \frac{(1+\zeta)^{4/3} + (1-\zeta)^{4/3} - 2}{2^{4/3} - 2} \tag{2.15}$$

The explicit spin dependence exchange-correlation potential is given

$$V_{xc,\alpha}(r) = \frac{\partial[n(r)\varepsilon_{xc}(n(r), \zeta(r))]}{\partial n_\alpha(r)} \qquad \alpha = \uparrow, \downarrow \tag{2.16}$$

thus splitting into two orthogonal subspaces.

For the set of $\{\phi_{i\alpha}^0(r)\}$ which minimizes the energy functional (2.9), $n(r)$ and $\zeta(r)$ coincide with the true ground state density $n_0(r)$ and spin

polarization $\zeta_0(r)$ of the system respectively, while E becomes equal to the ground state energy $E_0(\{R\})$.

Finally the ionic motion is described by classical equations similar to Eq.(2.3)

$$M_I \ddot{R}_I = -\frac{\partial V_{II}}{\partial R_I} - \int dr n_0(r) \frac{\partial V_{eI}(r, \{R\})}{\partial R_I} \tag{2.17}$$

We solve the coupled set of Eqs.(2.8) and (2.17) using techniques similar to those described in the previous section for the single electron case. Due to the unitarity of the approximate formula (2.6), if the wavefunction $\psi_{i\alpha}$ are initially orthogonal, they will maintain this property during all subsequent time evolution. For a system of two electrons, this remark is particularly relevant in the case of parallel spin electrons where orthonormality of the $\psi_{i\alpha}$ is a necessary consequence of the Pauli principle. The time step to be chosen to integrate the equation (2.8) is $\Delta t \sim 0.5 a.u.$, while for the ionic motion the time step $\Delta T = 20 \times \Delta t = 10 a.u.$. In one of our runs, we used $\Delta t = 0.4 a.u.$ to maintain the conservation of the total energy.

Chapter 3

Model Calculations

In this chapter we describe in detail our calculations for a model of electrons solvated in NaBr.

3.1 MD cell and representation of the electronic wavefunction

In our system periodic boundary conditions are imposed, each unit box containing 32 Na^+ cations and 31(30) Br^- anions and 1(2) electron(s) in order to keep the system neutral. We represent each wavefunction on a discrete mesh of 16^3 points in the cubic Molecular Dynamics (MD) cell of length $\sim 25.4 a.u.$. Such a small simulation box was found adequate for the study of most properties, since, as we shall see, the electron states are usually well localized. Fourier transforms used to switch to reciprocal space, are performed using 16^3 reciprocal lattice vectors, i.e., all the G vectors compatible with the choice of the mesh in direct space.

3.2 Potentials

a) Ion-ion interactions

In the case of the alkali halides the interionic forces are predominantly coulombic and each ion is usually assumed to have a charge numerically equal to the charge on an electron. The other important term in the interionic potential is that describing the short-range repulsion, which arises physically from the 'overlap' forces between ions. We take the Born-Meyer potential [35]

$$\Phi_{ij}(r) = c_{ij} b e^{(\sigma_i + \sigma_j - r)/\rho} + \frac{Z_i Z_j e^2}{r} \tag{3.1}$$

where b is the same for all salts, σ_i and σ_j are lengths characteristic of the ion i and j, ρ is a 'hardness parameter' characteristic of the particular salt, and c_{ij} are the numerical coefficients introduced by Pauling. Z_i and Z_j are the ionic charges. The calculation of the parameters in the repulsive terms has been carried through by Tosi and Fumi [36] for all the alkali halides. The calculations were made by fitting experimental crystal data. For NaBr salt the parameters are: $b = 3.38 \times 10^{-3} erg, c_{++} = 1.25, c_{+-} = 1.00$ and $c_{--} = 0.75$, $\sigma_+ = 1.170(\mathring{A}), \sigma_- = 1.716(\mathring{A})$, and $\rho = 0.340(\mathring{A})$.

We treat the short-range part of the ion potential in real space, while the long-range part was treated by Ewald summation method in reciprocal space.

b) Electron-ion interactions

The electron-ion pseudopotentials were taken to be a smoothed version of those used in Ref.[10], i.e.

$$v_{e,\pm} = \mp \frac{1}{r} erf(r/R_\pm) \tag{3.2}$$

where the core radius $R_+ = 3.0a.u.$ for Na^+ and $R_- = 2.2a.u.$ for Br^-. Such smoothing is required by our use of a discrete mesh to represent the wavefunction ψ and does not introduce any significant quantitative effect. The R_- is not physically meaningful but is just a cutoff radius which is again related to the use of a discrete spatial mesh. Reasonable variations of this value leave our results unchanged. The

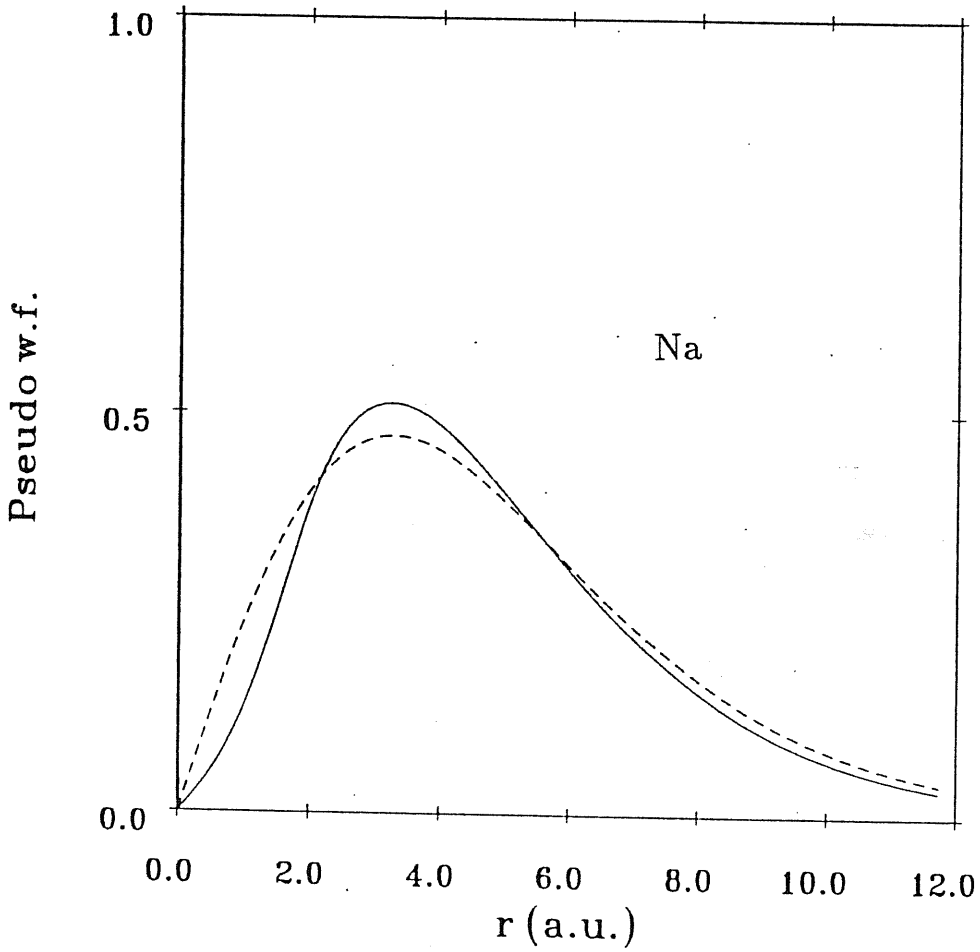

Figure 3.1: $3s$ pseudo-wavefunctions for Na, obtained using the *ab initio* pseudopotential of Ref.[38] (solid line) and our model potential (dashed line).

core radius for Na^+ is chosen to approximately fit the atomic ionization potential. With the form (3.2) of our electron-ion pseudopotential, the value $R_+ = 3.0 a.u.$ is found more appropriate than the value $3.2 a.u.$ commonly used in Heine-Abarenkov pseudopotentials[37]. The resulting atomic $3s$ pseudofunction is reasonably close to that given by *ab initio* pseudopotential [38] (see Figure 3.1).

3.3 Preparation of the initial state

An important feature of the calculations is the preparation of the initial state. First of all we prepare a well equilibrated liquid of 32 Na^+ and

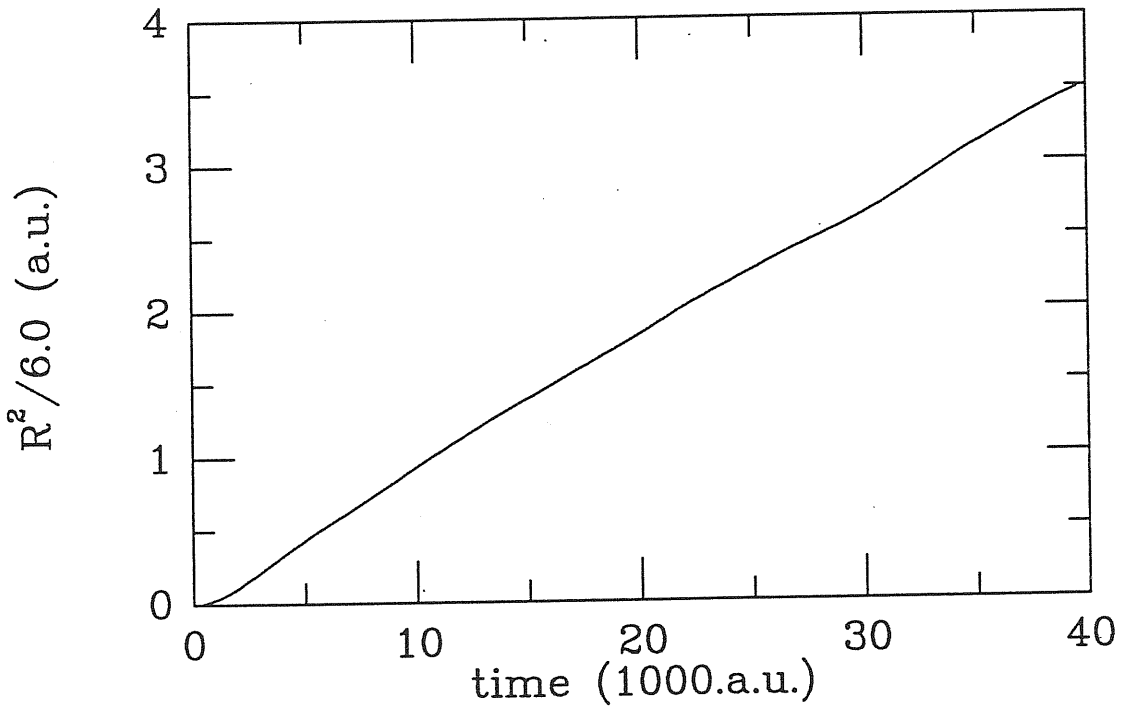

Figure 3.2: Time dependence of the ionic mean square displacement, obtained using 20 starting points in an ionic trajectory of run 240,000a.u.

31(30) Br^- in a neutralizing uniform background at temperature of about 1250K and density of 2.3 g/cm^3 for both cases. We start from a crystal supercell where 1(2) Br^- ion(s) are substituted by a negative charge background with the same total charge. We heat this system by rescaling the velocities of the all ions, the temperature being simply related to the average ion kinetic energy.

To check whether the system is in the liquid state, we follow the mean square displacement of the ions

$$R^2(t) = \lim_{T\to\infty} \frac{1}{TN_I} \int_0^T dt' \sum_I [R_I(t'+t) - R_I(t')]^2 \qquad (3.3)$$

where N_I is the total number of ions and summation is over all ions. In a liquid the value of the mean square displacement increases with time. As shown in Figure 3.2, the long-time part of $R^2(t)$ is approximately linear, indicating a diffusive motion. By using the Einstein formula

$$D_I = \lim_{t\to\infty} R^2(t)/6t \qquad (3.4)$$

we can obtain the diffusion coefficient $D_I \sim 1.0 \times 10^{-4} cm^2/s$. The radial pair correlation function $g_{(Na^+-Br^-)}(r)$ between positive and negative ions, as well as the pair correlations between all positive ($g_{(Na^+-Na^+)}(r)$) and all negative ($g_{(Br^--Br^-)}(r)$) ions are shown on Figure 3.3. They are very similar to the pure molten salt pair correlations and exhibit the characteristic alternation of positively and negatively charged shells. This is to be expected here since the electron concentration ($x = 0.031$ and 0.062 for the single and two electron case, respectively) is very low.

A typical liquid configuration was stored, and for such a fixed ionic configuration we remove the uniform background and calculate the ground

state of the 1(2) electron(s) system. The ground state eigenvalue E_0 and eigenfunction ϕ_0 of the electrons were determined in the different way for the one and two electron cases, respectively.

For the system of 32 Na^+, 31 Br^- and one electron, we calculate the

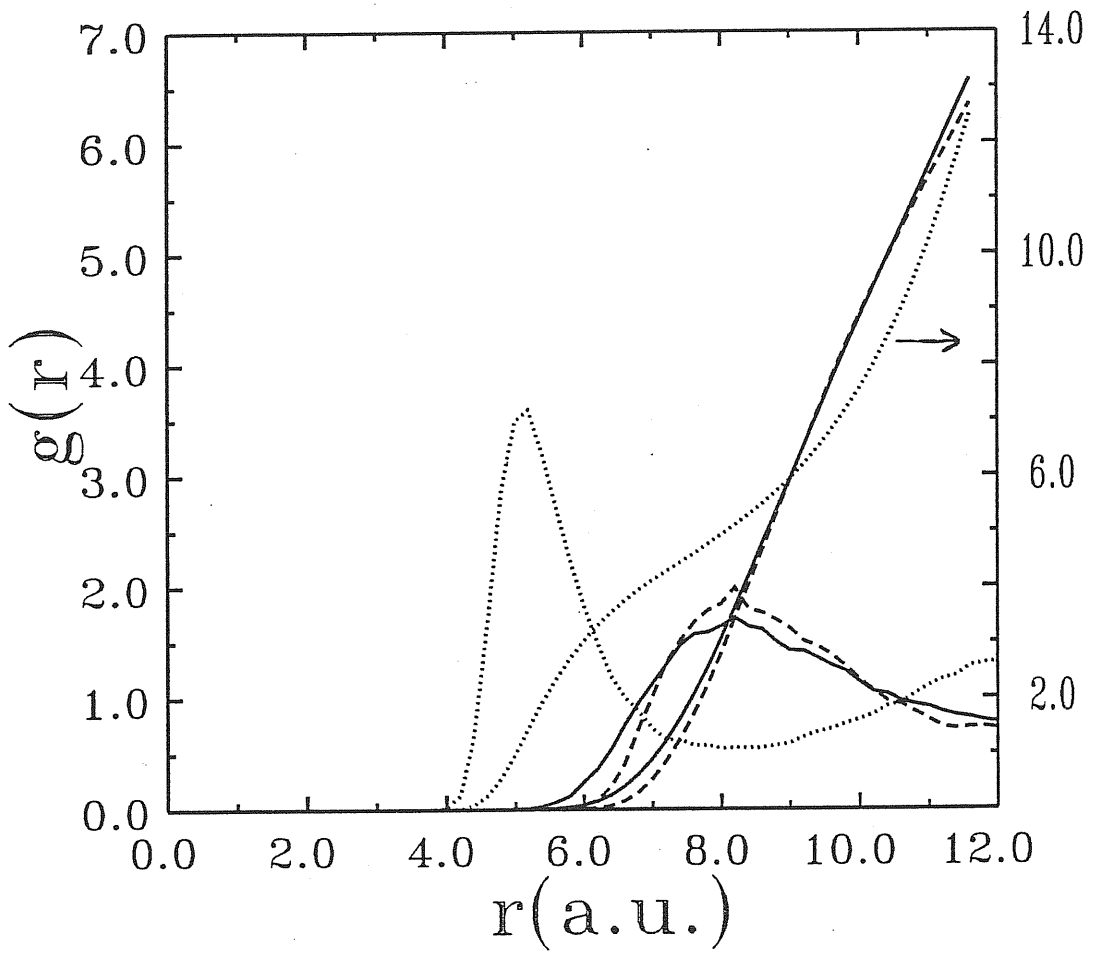

Figure 3.3:

Radial ion-ion pair correlation functions $g_{(Na^+-Br^-)}(r)$ (dotted line), $g_{(Na^+-Na^+)}(r)$ (solid line) and $g_{(Br^--Br^-)}(r)$ (dash line) in molten salt Na-NaBr. On the right scale the corresponding coordination numbers are also indicated.

ground state of the Hamitonian $H(\{R(t_0)\})$ by standard diagonalization using a plane wave basis set. Due to the smoothness of our electron-ion

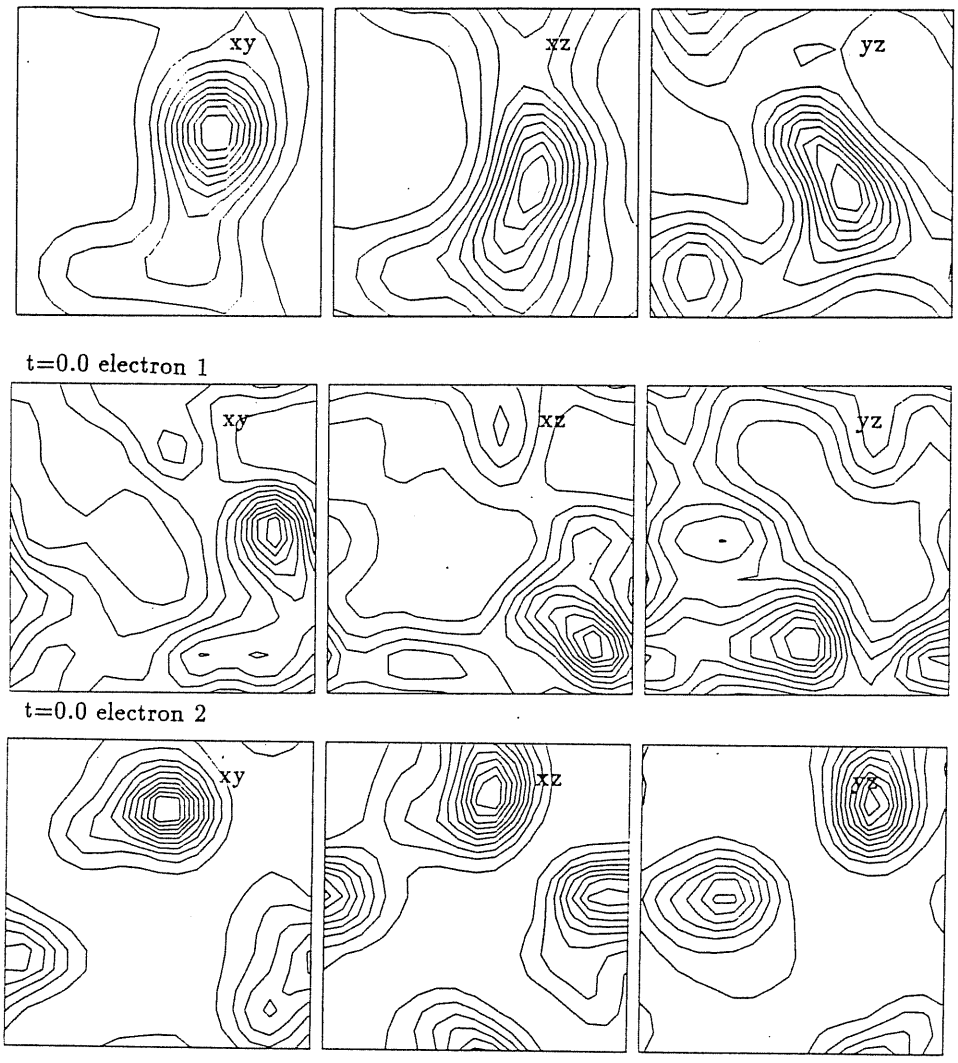

Figure 3.4:

Charge density contour plots for the initial states of our run integrated along z(left), y(center) and x(right). Top panels: one electron case. Middle and bottom panels: two electron case.

pseudopotentials, we found that a kinetic energy cut-off of the order of 2 Ry, which corresponds to 500-600 plane waves, is sufficient to ensure very good convergence. For the system of 32 Na^+, 30 Br^- and two antiparallel spin electrons, the ground states were calculated by minimizing the energy functional (2.9) with Steepest Descent(SD)[39] and/or Conjugate Gradient(CG) [40] (see Appendix B) methods. The CG is much more rapidly convergent. The criterion we used to ensure the convergence is that the energy difference between two sequence steps is less than $10^{-7} a.u.$. The contour plots of the integrated electronic charge density $\rho(x,y) = \int dz n(x,y,z)$ *etc.* for the initial state of one and two electron cases are shown in Figure 3.4. The ground state $\phi_0(\{R(t_0)\})$ of the electrons together with the stored ionic configuration $\{R(t_0)\}$ were used as the initial conditions for running our dynamics.

3.4 Initial dynamics

a) Single electron

Initially the electronic energy $E = < \psi | H_{eI} | \psi >$ decreased steadily. This was found to correspond to an adiabatic localization of the electron from an initial fairly delocalized state into a well localized state. This is indicated by the behavior of the participation ratio [41]

$$p = [\Omega \int_{\Omega} dr |\psi(r)|^4]^{-1} \tag{3.5}$$

which is a measure of the localization of the particle wavefunction ($0 \leq p \leq 1$, where $p = 0$ and 1 for a perfectly localized and delocalized state respectively). The value the participation ratio changed from the initial value ~ 0.12 to ~ 0.025 at time 15,000 $a.u.$ in our case. In Fig. 3.5 we

show the typical charge density of the ground state of our run, which is s-like, and that of the first excited state, which is p-like.

b) Two electrons with antiparallel spins

For two antiparallel spin electrons no constraint must be imposed to satisfy Pauli's exclusion principle. Initially the electrons localized to form two distinct localized states from the initial quite delocalized ones. By the time 25,000 *a.u.*, the two electrons with antiparallel spins have paired, giving arise to a single-center localized state which is more spread out than single electron state. These qualitative feature are sum-

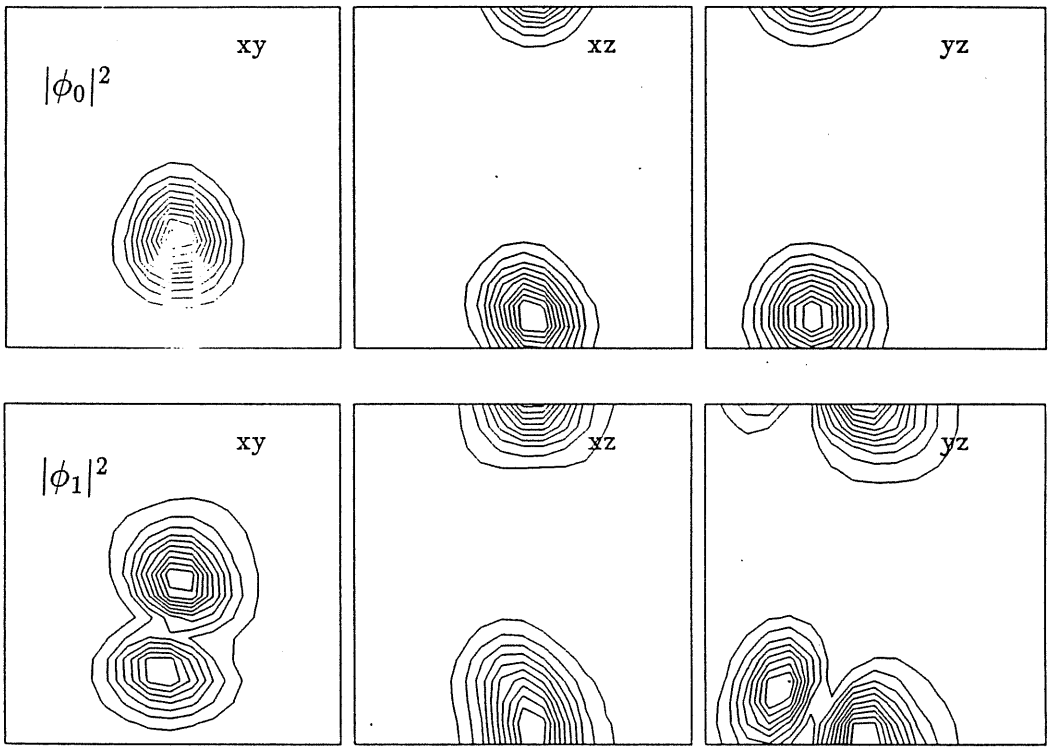

Figure 3.5:

Top panel: Contour plots of the electronic density of the ground state ϕ_0 for a typical configuration. Bottom panel: the corresponding first excited state ϕ_1.

marized in Fig. 3.6 where we show contour plots of the charge density $\rho(x,y) = \int dz n(x,y,z)$ *etc.* at time 15,000 *a.u.* (when the two electrons are separated) and 25,000 *a.u.*. (when the two electrons are paired).

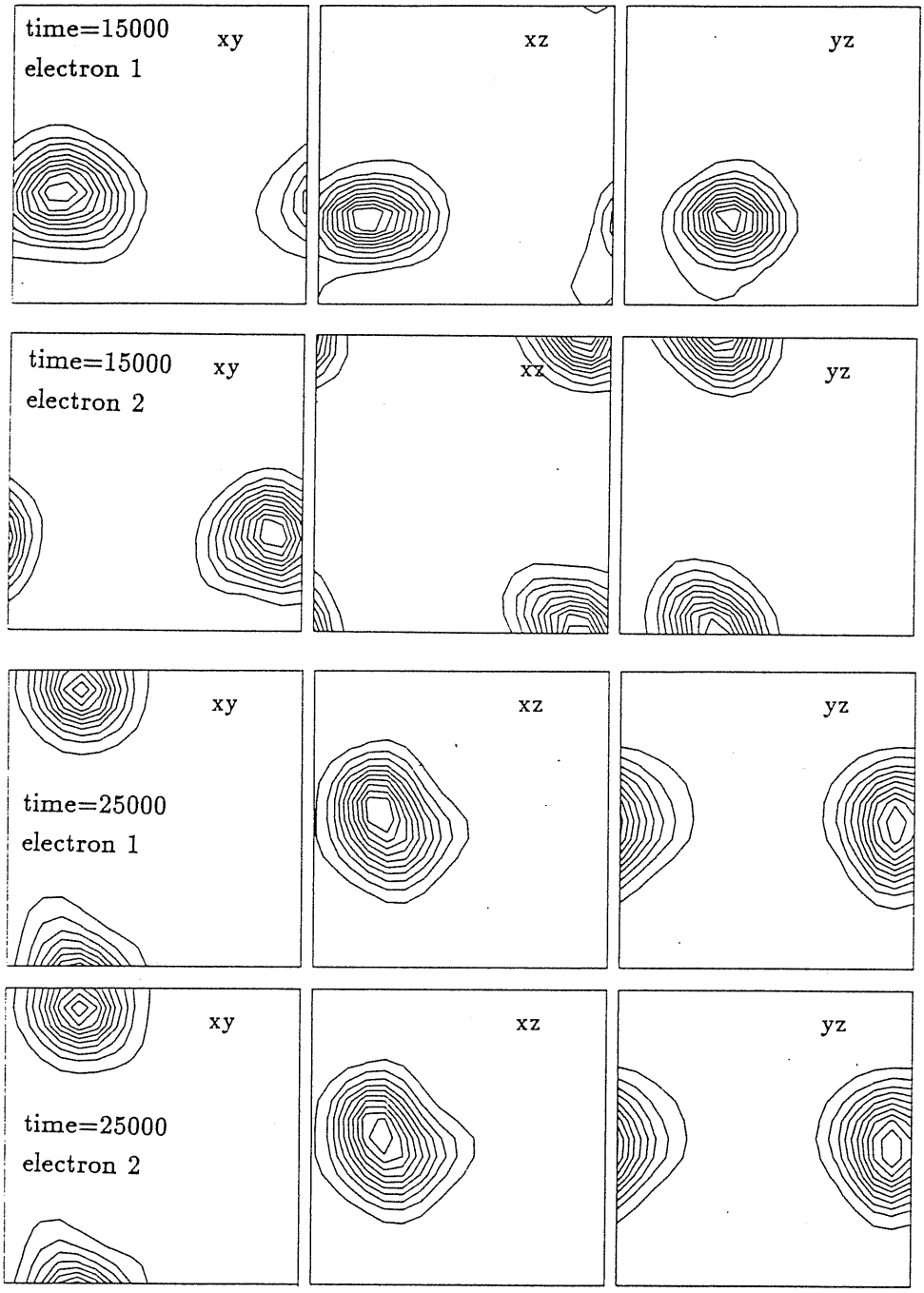

Figure 3.6: Contour plots of the projected electronic density of the two paired electrons at time 15,000 *a.u.* (upper panels) and 25,000 (lower panels).

Chapter 4

Structure of Electronic States in Dilute Na-NaX Solutions

In this chapter we describe the structure of one and two electron states in dilute Na-NaBr solutions and compare it to that in K-KCl solutions.

4.1 Single electron: dipolar atom

a) Electron-ion correlation functions

In order to characterize the electronic structure and the ionic distribution around the localized electron, we introduce the following pair correlation functions between the electron and the Na^+ and Br^- ions

$$g_{e,\pm}(r) = \frac{\Omega}{4\pi r^2 N_e N_\pm} < \sum_{I_\pm} \int dr' n(r') \delta(|r' - R_{I_\pm}| - r) > \qquad (4.1)$$

Here Ω is the volume of the simulation box, N_e the number of electrons, and $N_+(N_-)$ the total number of cations (anions) to which the

sum over $I_+(I_-)$ is extended, and the bracket indicates temporal average.

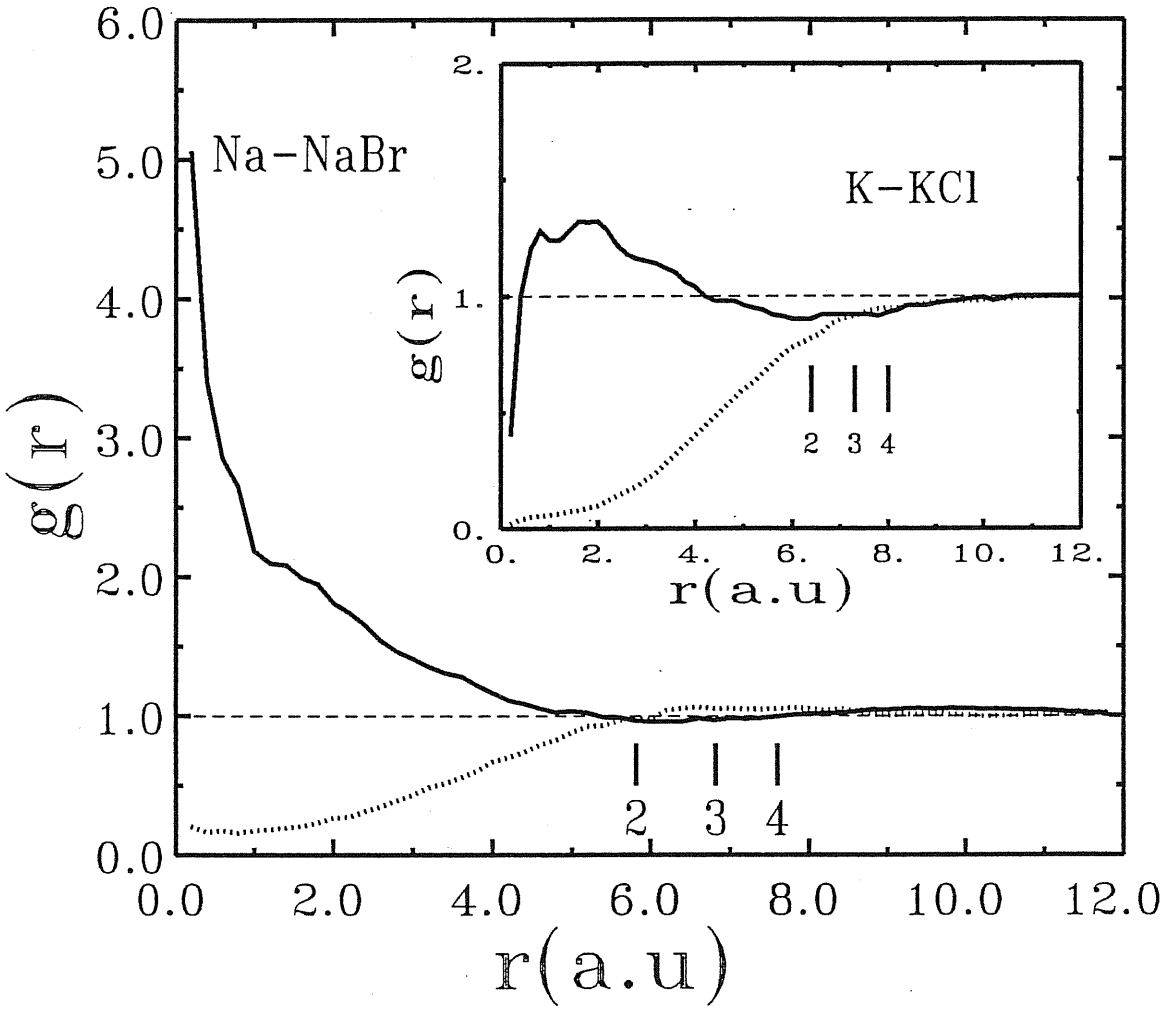

Figure 4.1:

Electron - cation (full line) and electron - anion (dashed line) radial pair correlation functions for an electron in NaBr. In the inset are the results of a similar calculation for an electron in KCl at $\sim 1200K$.

The functions (4.1) are displayed in Fig. 4.1. In the inset we also show, for comparison, the same quantity for K-KCl. It is apparent that in both cases the electron is localized in a region where the probability of finding an anion is very low. However a substantial difference of electron-cation correlation function between Na-NaBr and K-KCl is evident, and in particular it is clear that the electron states in NaBr are much more localized and atomic-like than in KCl. Also indicated in Fig. 4.1 are a few values of the coordination function

$$Z_+(r) = \frac{4\pi N_+}{\Omega} \int_0^r g_{e,+}(s) s^2 ds \tag{4.2}$$

from which we may roughly estimate that the average coordination number Z_+ is between 2 and 3 in NaBr, whereas the corresponding number for the F-center -like state in KCl is $Z_+ \sim 4$.

b) Ionic trajectories in proximity of the electron

Since the electron is on average well localized, we can define the center of mass W of the electron . In order to determine W, one has to first to define the position operator $\hat{r}$ for a periodic system. A possibility which works well for localized wavefunctions is to define the expectation values $< \hat{r} >$ as follows [20,42]

$$< \hat{r}_\alpha >= \frac{L}{2\pi} Im(ln < \phi | e^{i2\pi \hat{r}_\alpha / L} | \phi >) \tag{4.3}$$

$$\alpha = x, y, z$$

where L is the size of the unit box (which we assume cubic) and $\hat{r}_\alpha$ is the standard definition of the position operator.

Using Eq.(4.3), we calculate first the center of mass W of the wavefunction ψ and then calculate the relative distance between the center

of mass and the ions closest to it. In Fig. 4.2 we show the typical time evolution of the distance ($\leq 9a.u.$) during one of our runs. For comparison, in the right panel of Fig. 4.2 a similar plot for K-KCl is also given, showing typical F-center configurations. It appears that the con-

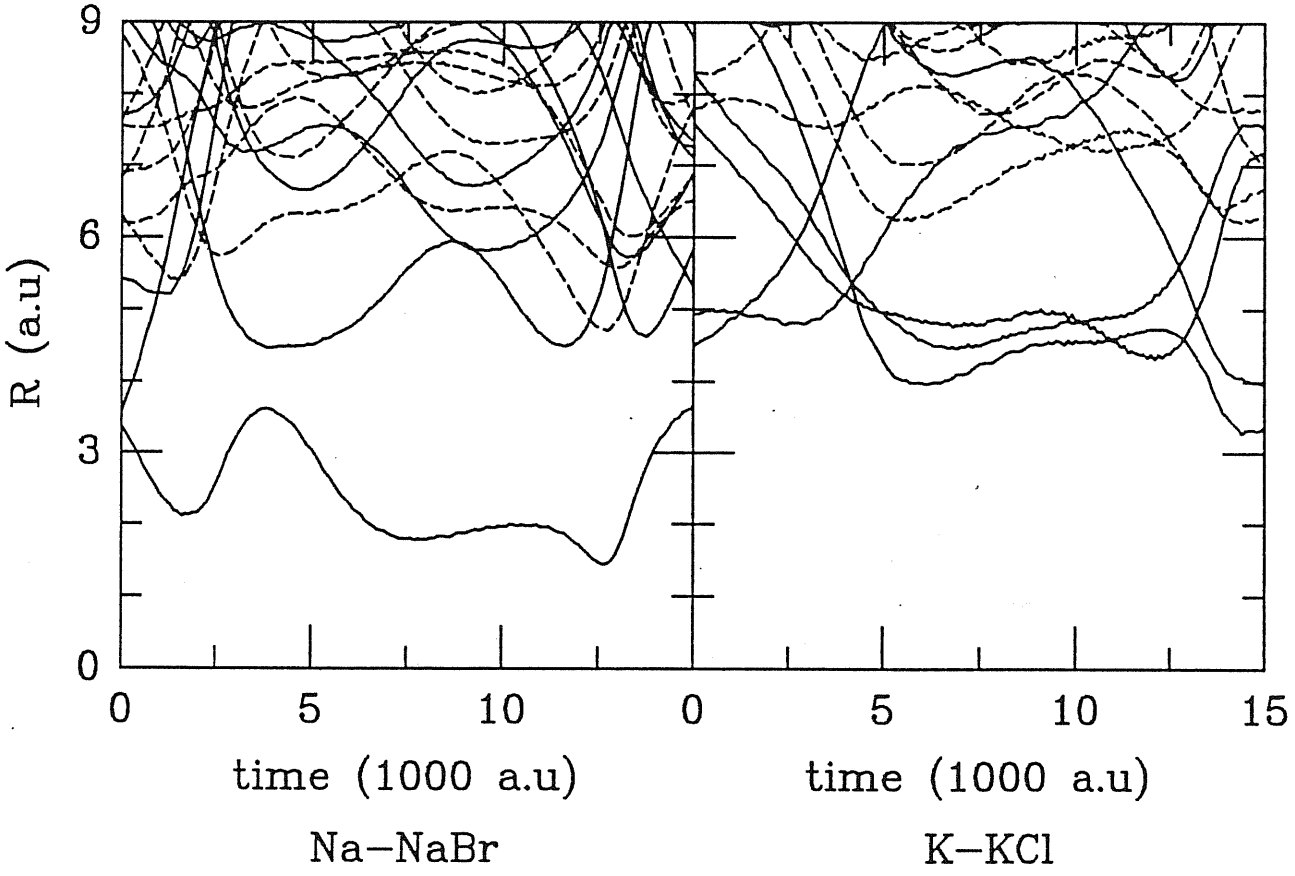

Figure 4.2:

Typical time-evolution of the distance between the center of mass of the electron and the ions closest to it. The trajectories of the cations (anions) are drawn as full (dotted) lines. Left panel: Na-NaBr. Right panel: K-KCl.

figurations in NaBr are typically atomic-like, i.e. there is a single Na^+ ion which is much closer to the electron than all the others, clarifying the origin of the low coordination number Z_+ in Na-NaBr. However, Na_2^+-molecular-like (see Fig. 4.3.) and F-center-like configurations are also observed. In the atomic-like configuration, the distance between Na^+ and the electron is of the order $\sim 2 - 2.5 a.u.$, whereas the next Na^+ neighbors sit at distance of $\sim 5 a.u.$ or more. For the F-center in KCl, in contrast, the distance between the electron and the cations of the first solvation shell is typically in the range 4 - 8 $a.u.$, as illustrated in the right panel of the Fig. 4.2.

c) Dipolar-atomic states

In the atomic-like configurations there is a strong admixing of p state into the s atomic state, which leads to the formation of a dipole moment. The mechanism for stabilizing the hybrization is provided by the solvent electric polarization induced by the atomic dipole. This mechanism, suggested by Logan [21,23], has been shown to be operative in a variety of situations.

The total energy ΔE of such a dipolar atom relative to the atomic non-polar state, after a simple manipulation of the formulas given by Logan, can be expressed in terms of the fraction f_p of p-character in the electron wavefunction as (A detail description see Appendix C)

$$\Delta E = -E_0 \frac{f_p^2}{(1 - 2f_p)} \tag{4.4}$$

where $E_0 = E_p - E_s$ is the atomic excitation energy. Correspondingly, the dipole moment μ is given by

$$\mu = 2M\sqrt{f_p(1 - f_p)} \tag{4.5}$$

where $M =< s|ex|p >$ is the intra-atomic matrix element of the dipole operator ex. For our dipolar atomic states in NaBr the projections of the electron wavefunction onto the s and p states centered on the nearest Na^+ ion are given in Fig. 4.4. These are typically $f_s \sim 0.75$ and $f_p \sim 0.2$. Using this value of f_p together with $E_0 = 2.1eV$ and $M \sim 8\ D$ in Eqs.(4.4) and (4.5), we obtain $\Delta E \sim -0.14eV$ and $\mu \sim 6.4\ D$. The latter value is in reasonable agreement with the dipole moment

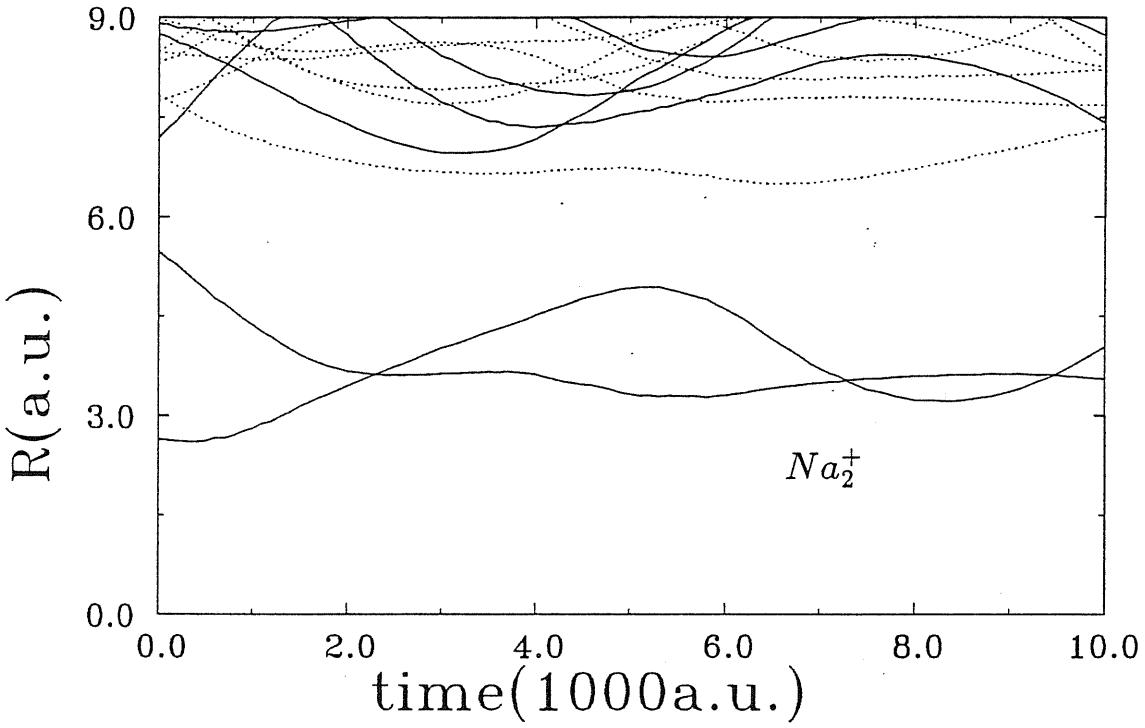

Figure 4.3: Ionic trajectories in proximity of the electron showing a Na_2^+- molecular-like state. The trajectories of the cations (anions) are drawn as full (dotted) lines.

of $\sim 5-6\ D$ which is estimated using the observed average distance $\sim 2-2.5\ a.u.$ between the center of mass of the electron and the closest Na^+ ion. We note that the dipolar atom can be continuously changed

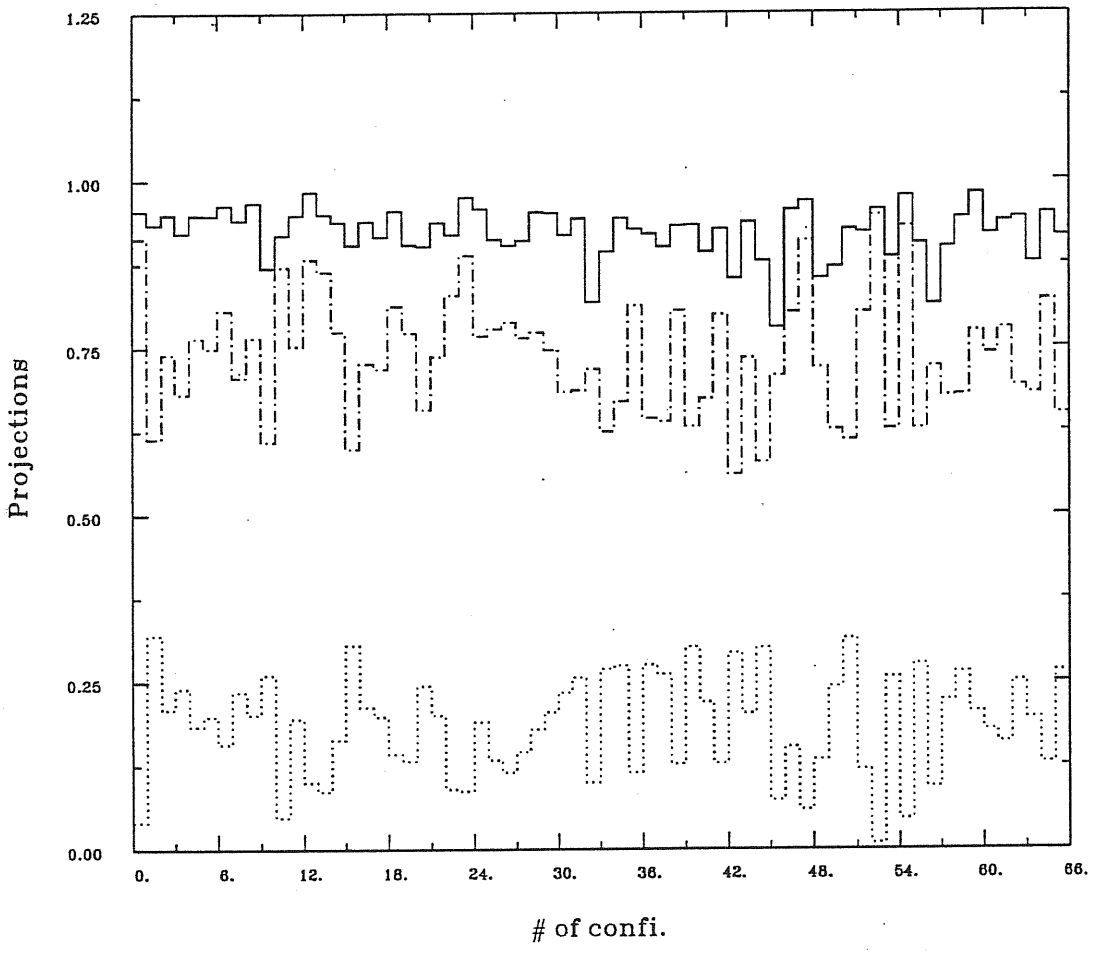

Figure 4.4:

Projections of the electron wavefunction onto the s (dotted-dash line) and p (dotted line) states centered on the nearest Na^+ ion for 66 configurations spaced by $5000 a.u.$ in time. The line is just a guide for the eye. The summation of the s and p states is plotted as a solid line.

into the F-center state upon increasing the amount of hybridization into the higher excited states.

For typical F-center configurations in KCl in fact the projections of the electronic wavefunction on the nearest cation are $f_s \leq 0.6$ and $f_p \geq 0.3$. It is interesting to note that also the highly simplified expression (4.4) for ΔE predicts a breakdown of the dipolar atom picture for $f_p \rightarrow 0.5$.

The key parameter which appears to control the relative stability of the dipolar atomic state vs. the F-center in our calculations is the strength of the electron-cation potential, which determines, in particular, the values of the excitation energy and ionization potential of the metal atom. We have indeed verified that the dipolar atomic state of NaBr evolves gradually to an F-center state when the Na^+-potential is changed abruptly to that of K^+ (with all the other parameters of the calculation left unchanged), in agreement with the results of similar Path-Integral calculations [10].

4.2 Two electrons: spin paired species Na^- and Na_2

We performed calculation for the two electrons with paired spins. Paramagnetic susceptibility measurements [9] indicate that as the solvated electron concentration increases, spin pairing becomes operative. Similarly, numerical PI [24] and QMD [20] calculations for K-KCl solutions have shown that two antiparallel spin electrons attract each other and tend to form a bielectronic complex.

We used Eq.(4.1) to characterize the ionic distribution around the two antiparallel electrons in terms of radial pair correlation functions between the electrons and Na^+ and Br^- ions. The functions $g_{e,\pm}$ are

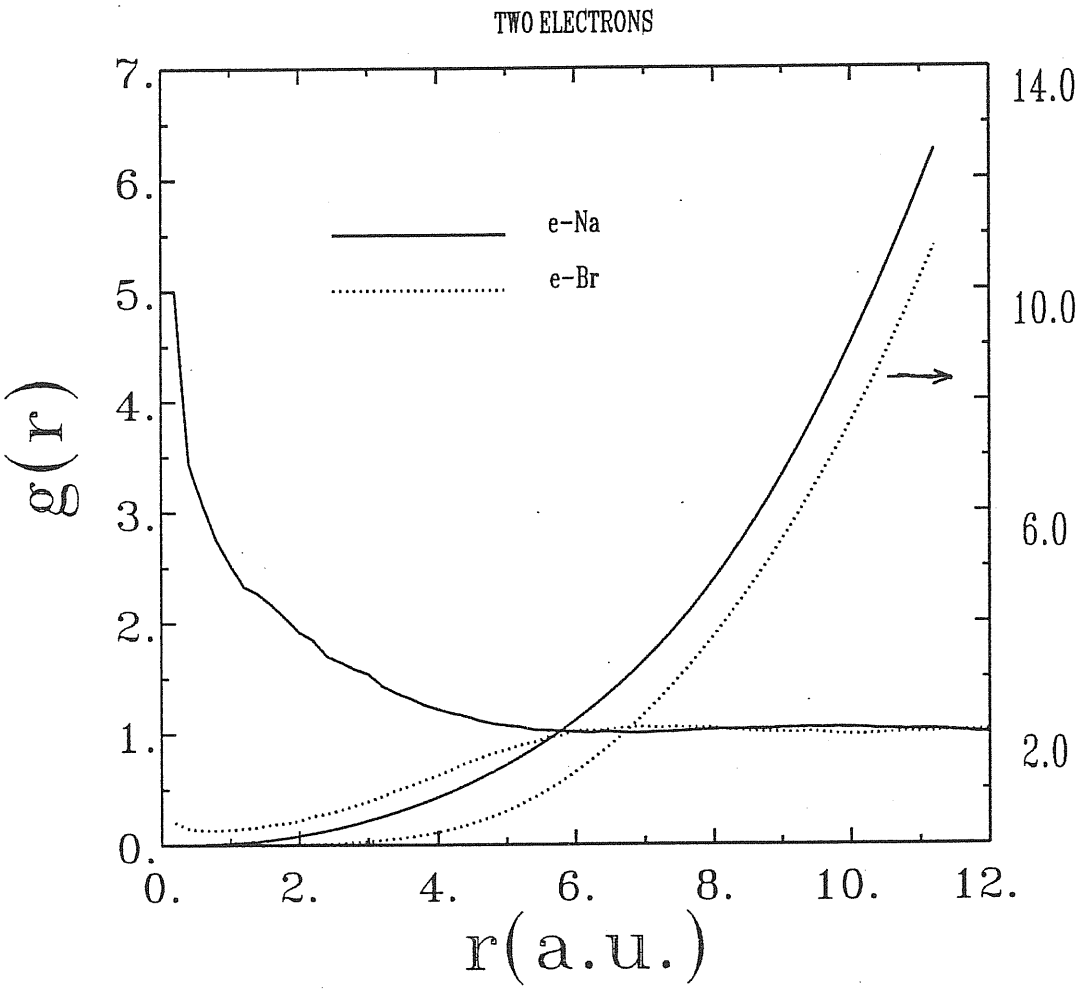

Figure 4.5:

Electron-cation (full line) and electron-anion (dashed line) radial pair correlation functions for two antiparallel electrons in NaBr. Curves referring to the scale on the right give the number of ions surrounding the electron.

shown in Fig. 4.5, which is substantially identical to that in Fig. 4.1 for the single electron case.

As in the single electron case, we have studied the time evolution of the distance between the centers of mass W_α of the two single-particle wave functions ϕ_α and the ions closest to these. These trajectories are shown in Fig. 4.6 for two electrons in the same time period. The analysis of the the ionic trajectories indicates that the two electrons are most frequently close to a single Na^+, thus forming a Na^- species with a pronounced dipolar character. Other species are also observed, most noticeably Na_2 molecular and bipolaron-like complexes where the two electrons sit in a fluid cavity which is surrounded by ~ 4 cations [20,24]. All these spin-paired species can change into one another via two different mechanisms. The first is due to the ionic diffusion which continuously causes the evolution of one species into another making the distinction between the two different species sometimes arbitrary. The second is more abrupt since it occurs via jumps similar to those in the one electron system. Such a situation is illustrated in Fig. 4.6, where the jump is indicated by an arrow. These jumps lead to dissociation of the current species followed by localization of the two electrons in different spatial positions. Recombination of the two electrons to form spin-paired species can also occur via jumps of one electron to the same spatial position of the other.

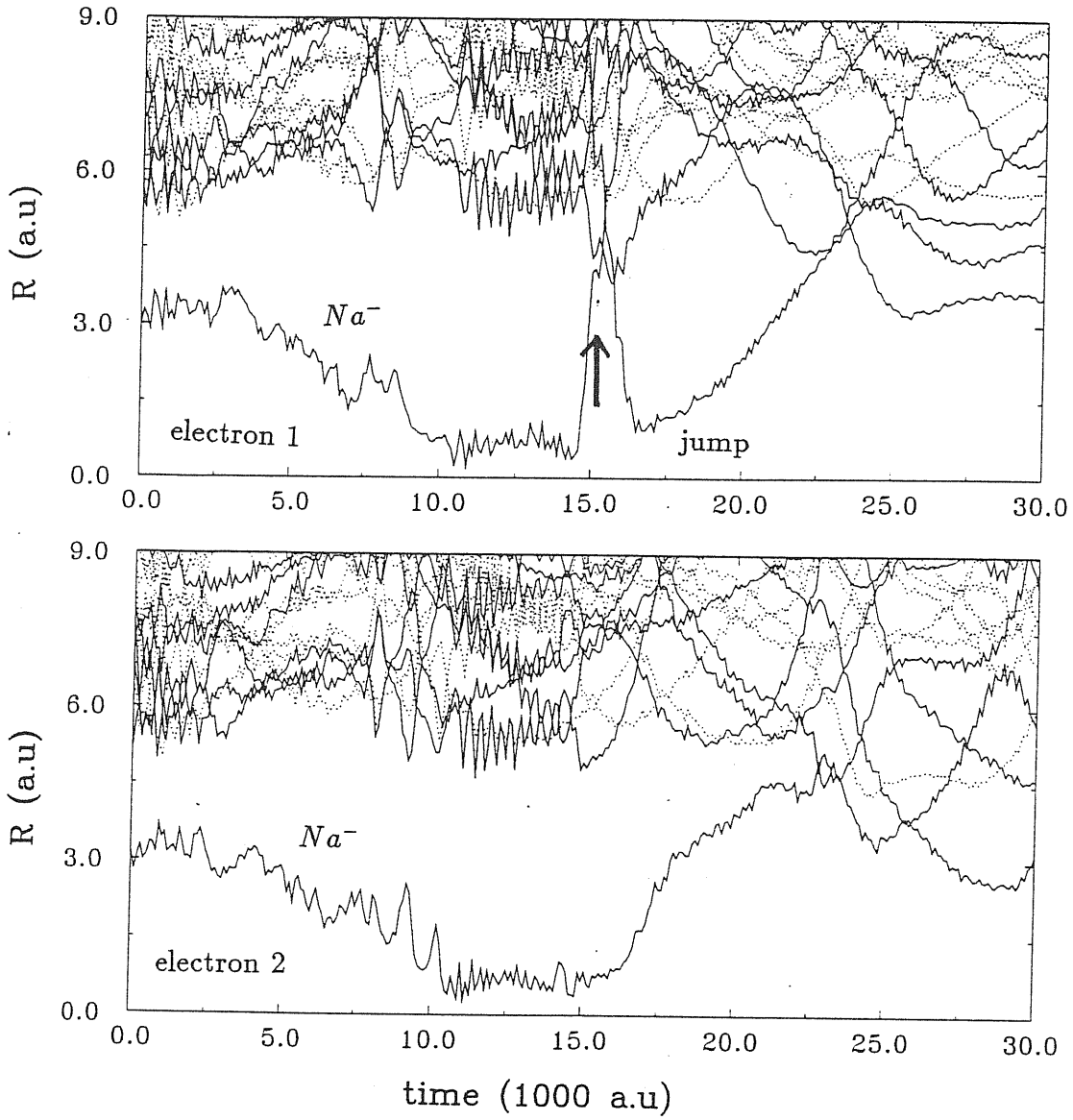

Figure 4.6:

Ionic trajectories in proximity of the two electrons with antiparallel spins during the same period. The trajectories of the cations (anions) are drawn as full (dotted) lines. Various species formed by the two electrons are also indicated. The noise of the curves shown is due to the fluctuations of the c.o.m. of the electrons. The arrow indicates a jumping event.

Chapter 5

Dynamical Properties: Optical Spectrum and Diffusion Coefficient

In this chapter we study the dynamics of the electrons and consider both short and long time scale properties, namely the optical spectrum and transport. In doing so, we shall neglect the non-adiabatic effects mentioned in chapter 2, which should not affect significantly such physical properties.

5.1 Optical absorption spectra

a) single electron case

We calculate the optical conductivity $\sigma(\omega)$, using the Franck-Condon approximation, i.e. evaluating the spectrum for a fixed ionic configuration and averaging over several different configurations. For a given

ionic configuration $\{R\}$, $\sigma(\omega)$ is given by the Kubo-Greenwood formula

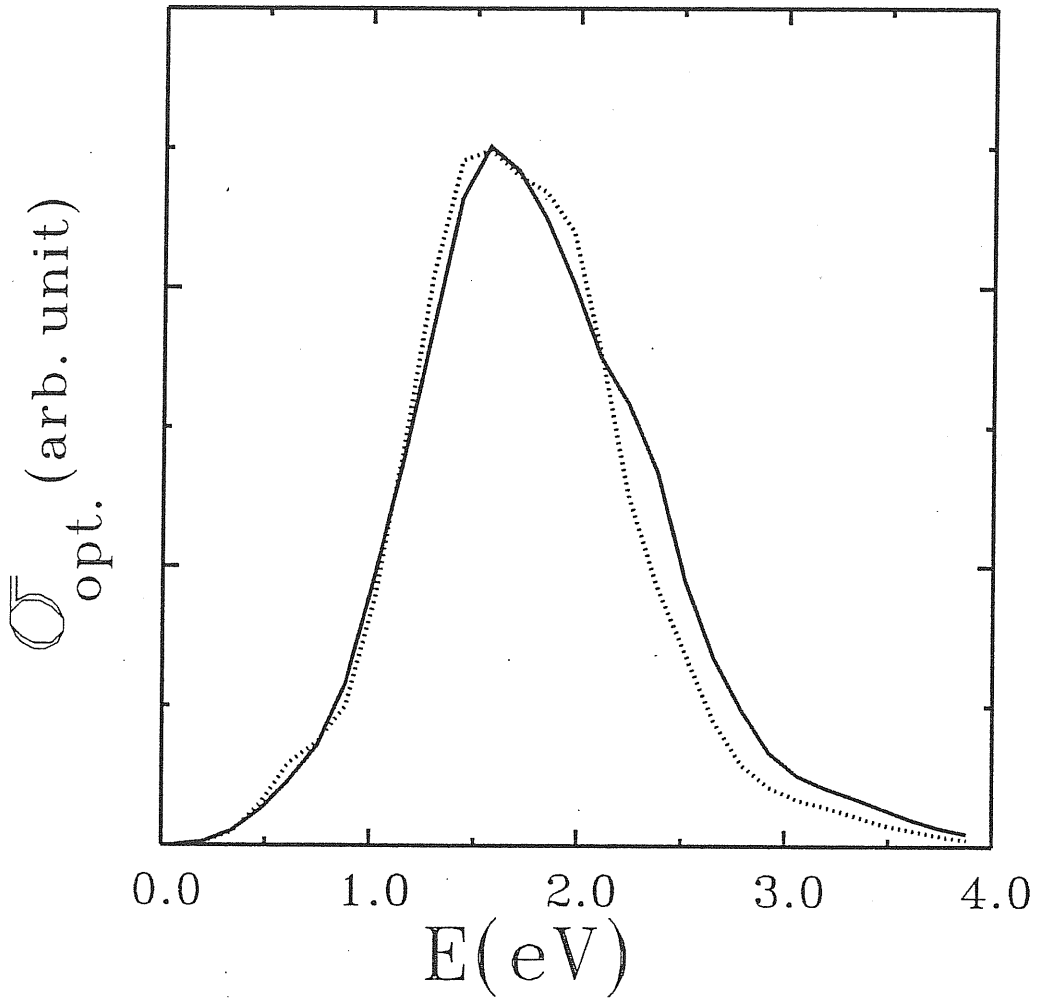

Figure 5.1:

Optical spectrum for Na-NaBr (solid line) and K-KCL (dashed line) at concentration $x \sim 3.1\%$. These spectra were calculated by averaging 83 and 60 configurations for NaBr and KCl, respectively. A Gaussian broadening of width $\delta = 0.136eV$ has been used in both cases. Curves have been normalized to the same area.

[43]:

$$\sigma(\omega) = \frac{\pi e^2}{m\omega}\frac{1}{\Omega}\sum_n | < \phi_n(\{R\})|v|\phi_0(\{R\}) > |^2 \delta(E_n(\{R\}) - E_0(\{R\}) - \hbar\omega) \tag{5.1}$$

where $v = -(i\hbar\nabla/m)$ is the electron velocity operator and the summation is extended to all excited state. In our calculations, we averaged over 80 different ionic configurations generated using Eqs.(2.2) and (2.3). Successive configurations differ by a time interval of $5000\Delta t$, which roughly corresponds to a typical ionic period. The eigenvalues and eigenstates were obtained by standard diagonalization using a plane wave basis set. The results of such a calculation are displayed in Fig. 5.1. The spectrum is dominated by transitions from the ground state (typically s-like) to the first few excited states (typically p-like). The gap in energy between ϕ_0 and ϕ_1 is usually > 1.0 eV, whereas all high excited states are quite close in energy. For comparison, the result of a similar calculation for the F center in KCl at 1200K is also shown in Fig. 5.1. It appears that the shape of the spectrum in NaBr is broader that in KCl, in agreement with the experiment [4].

b) two electron case

The calculation of the spectrum for the two-electron system has been performed in a similar way. If we assume that the KS wave functions and eigenvalues correspond to single-particle properties of our system, one can approximately calculate the optical conductivity as in the single electron system

$$\sigma(\omega) = \frac{\pi e^2}{m\omega}\frac{1}{\Omega}\sum_\alpha\sum_{v,c} | < \phi^0_{v,\alpha}|v|\phi^0_{c,\alpha} > |^2 \delta(E_{c,\alpha} - E_{v,\alpha} - \hbar\omega) \tag{5.2}$$

where $v(c)$ refers to occupied (unoccupied) KS states. The KS ground-

state and self-consistent potential were calculated by Steepest Descent[39] and/or Conjugate Gradients[40] methods. The excited states were obtained by matrix diaganalization. In Fig.5.2 we show the spectrum obtained from Eq.(5.2) averaging 60 different configurations equally spaced by $5000\Delta t$. Some noise is caused by our limited sampling.

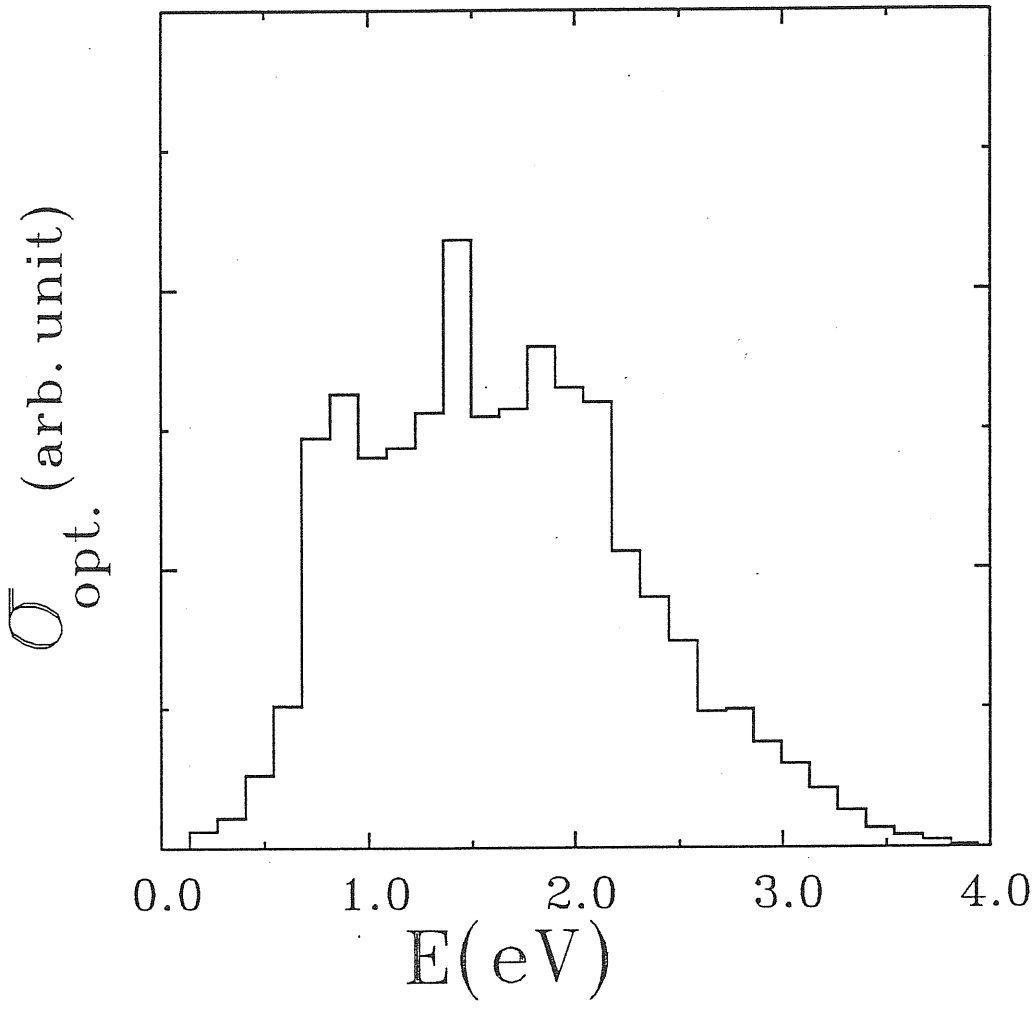

Figure 5.2:

Optical spectrum for Na-NaBr at concentration $x \sim 6.3\%$, calculated using the LSD approximation and averaging over ~ 60 configurations.

c) comparison with experiment

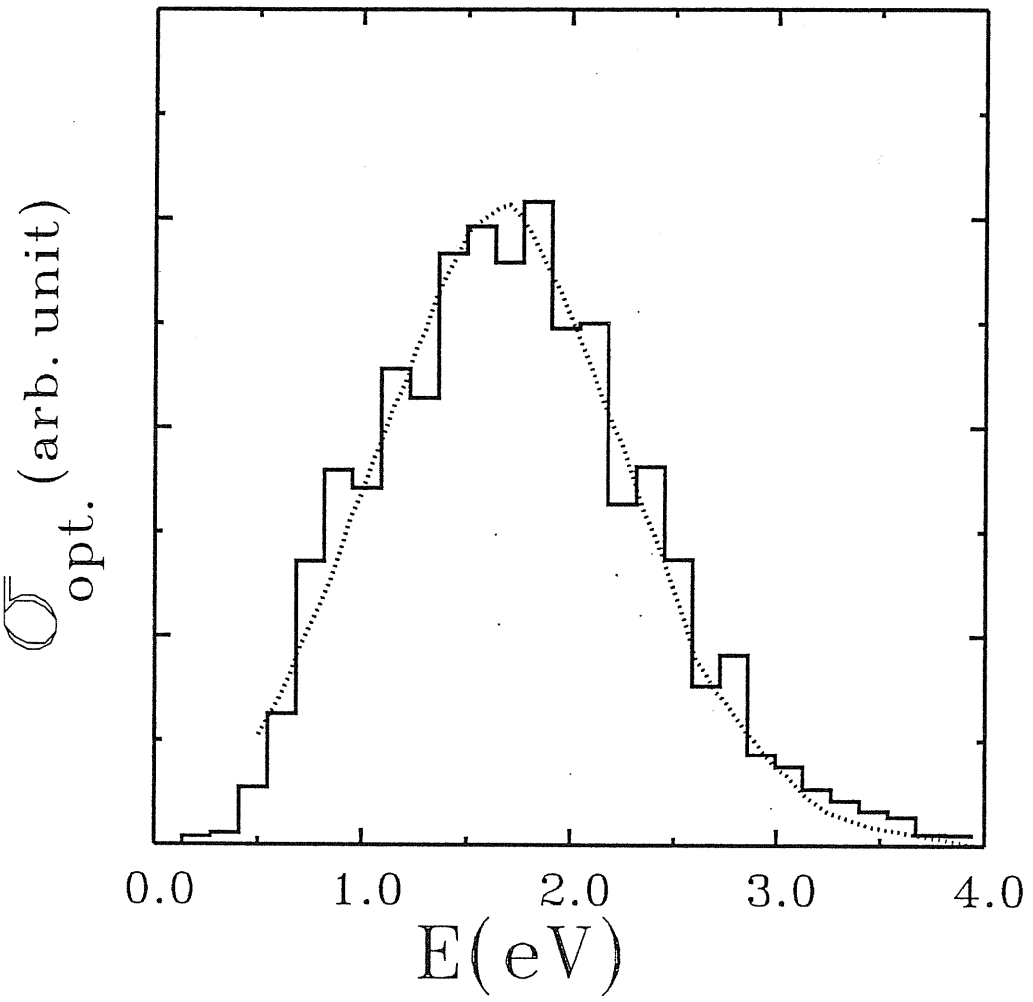

Figure 5.3:

Optical conductivity of Na-NaBr at metal concentration of 4.2%. The experimental (dashed line) and theoretical (full line) results have been scaled to the same height. The theoretical prediction for this concentration are obtained by linear combination between the calculated spectra for the one ($x \sim 3.1\%$) and two ($x \sim 6.2\%$) electron systems.

We have compared our results with the experimental data for an excess metal concentration of 4.2%. We obtained the theoretical predictions for the same concentration by linear interpolation between the calculated spectra for one ($x \sim 3.1\%$) and two ($x \sim 6.2\%$) electron systems. The results at $x \sim 4.2\%$ are shown in Fig.5.3. together with the experimental spectrum. The agreement between theory and experiment is remarkable. Although the calculated lineshape is obtained as an average of spectra that pertain to different configurations of the liquid, the experimental observation that the absorption band results from the superposition of two gaussian bands, can be tentatively related to the presence of dipolar-like states, where the p-like excited states split into a singlet and a doublet. The absorption peaks should correspond to transitions from the ground state to these singlet and doublet states. A simple estimate of their splitting has been given by Logan for the case of alkali atoms in rare gas solids[23]. In this case the splitting is $\Delta\omega = E_0 f_p/(1-2f_p)$ (see Appendix C). With our value $E_0 \sim 2\ eV$ we find $\Delta\omega \sim 0.4\ eV$ (the experimental separation between the two bands) for $f_p \sim 0.15$, which is in reasonable agreement with our calculated values for this quantity (see Fig 4.4).

5.2 Diffusion coefficient

In this section we consider the calculation of electronic transport properties, namely the electron diffusion coefficient D_e, for which the Franck-Condon approximation is no more adequate. Since in our problem the electron is most of the time well localized, we can calculate its mean

square displacement as

$$r^2(t) = \lim_{T\to\infty} \frac{1}{T} \int_0^T dt'[< r(t'+t) > - < r(t') >]^2 \qquad (5.3)$$

where $< r(t) >$ is the expectation value of the electron position, which is defined in Eq.(4.3) for a periodic system.

a) one electron case

Our result for $r^2(t)$ for the single electron case is shown in Fig. 5.4, which is averaged by choosing different times as starting points in a single electron trajectory. It is apparent that the long time behavior of $r^2(t)$ is approximately linear, indicating diffusive motion. Using Einstein formula $D_e = lim_{t\to\infty} r^2(t)/6t$ for the electron diffusion coefficient

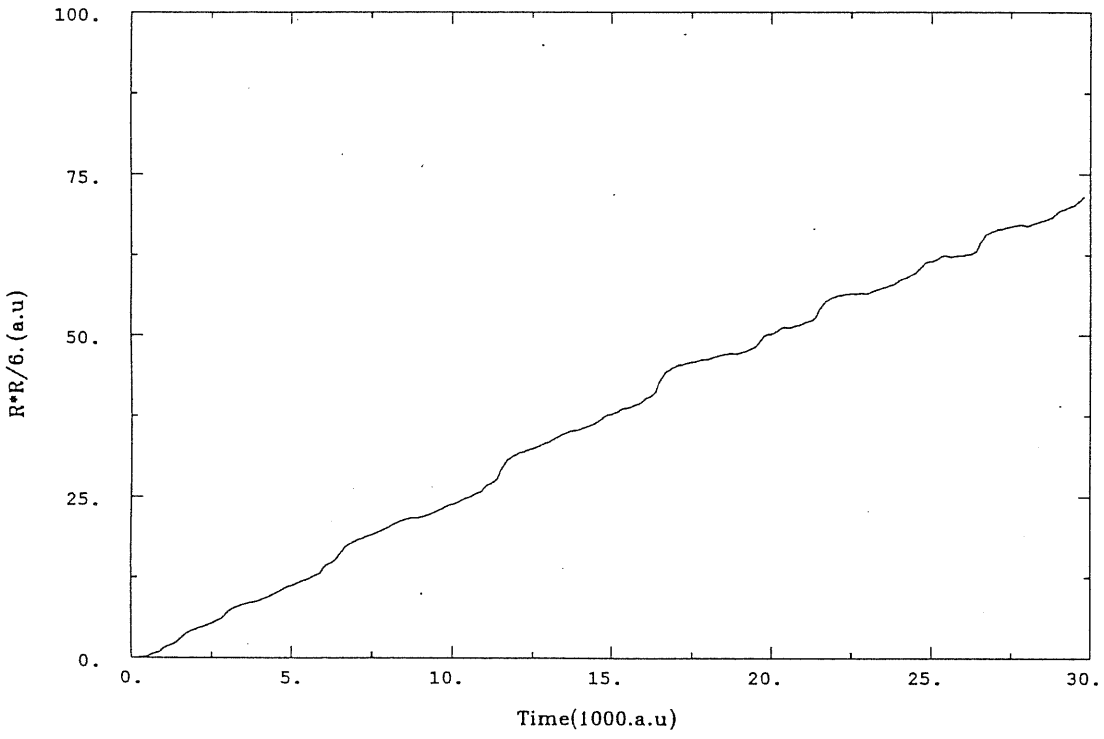

Figure 5.4: Mean square displacement of the electron as a function of time.

we find the value $D_e \sim 2.0 \times 10^{-3} cm^2 s^{-1}$. It is remarkable that in our calculation D_e is more than one order of magnitude larger than the ionic diffusion coefficient $D_I \sim 1.0 \times 10^{-4} cm^2 s^{-1}$, despite the fact that the motion of the electron is adiabatic. The high electronic diffusivity appears to be related to jumps between two spatially separated sites. Such jump are caused by the ionic diffusion which may successively make different sites in the liquid more favorable for the electron localization. During the hopping process the electron remains in the ground state, despite its wavefunction is quite delocalized, and the energy gap decreases substantially. It is possible that the gap becomes so small that transitions to excited states occur. This is the case in the rare non-adiabatic events. After this fast hopping process the electron becomes localized again.

b) two electron case

We follow the dynamics of the two electrons in a way similar to that for a single electron. The results of the mean square displacement are shown in Fig. 5.5. In both curves the long time behavior of $r^2(t)$ is approximately linear. We take the average of two values of diffusion coefficients and find $D_e \sim 1.5 \times 10^{-3} cm^2 s^{-1}$.

It is interesting to point out that the dissociation of the bielectron complex is usually related to the sudden jump of one of the two paired electrons, as indicated by an arrow in Fig.4.6. These jumps appear to be rather similar to those described above for a single electron. We did not observe events where both electrons of the paired species jump together from one localized states to another one in different place. Instead, the spin paired species moves smoothly, approximately on the same time scale of the ions.

c) electronic conductivity

These jumps are the essential mechanism that determines the electronic conductivity σ_e of our systems. The electron mobility is related to the diffusion coefficient by

$$\mu_e = \frac{e}{k_B T} D_e \tag{5.4}$$

From the electron mobility we obtain for $\sigma_e = n_e e \mu_e$ the values $\sigma_e \sim 1.0$ and 1.6 $\Omega^{-1}\ cm^{-1}$ for the one and two electron cases respectively. This corresponds to a sublinear increase of σ_e with electron concentration, in agreement with experiments[2]. This behavior is to be related to the fact that the mobility of the spin-paired species is very low, as indicated

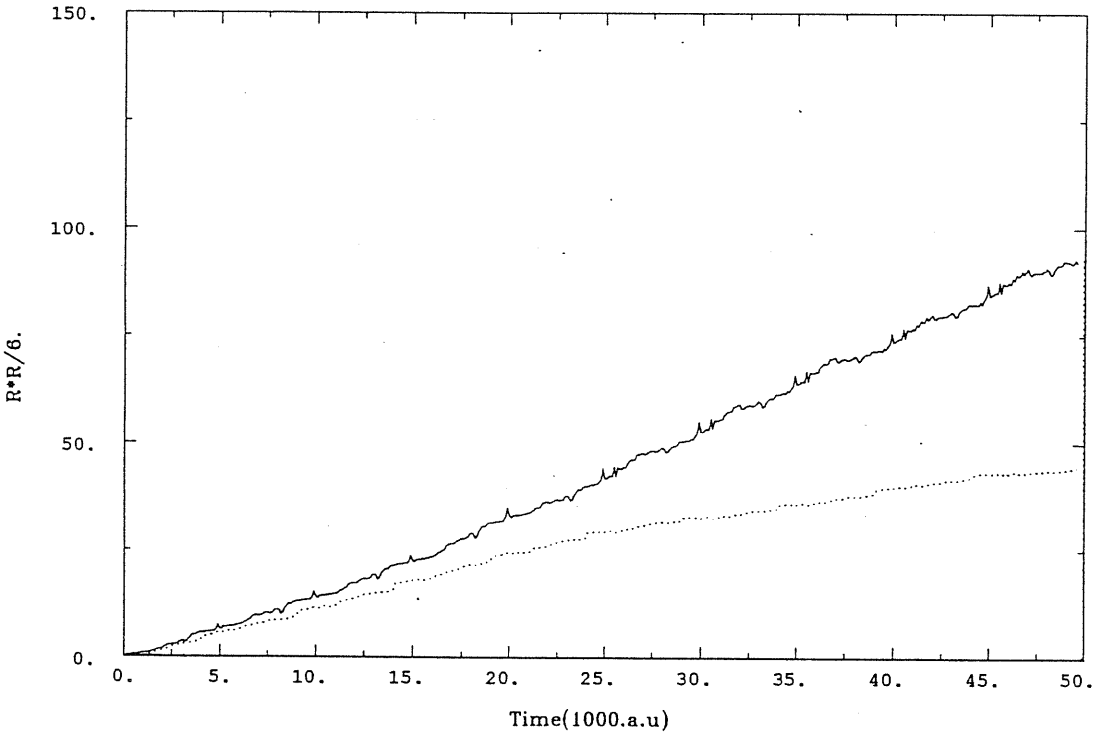

Figure 5.5: Mean square displacement of the two antiparallel spin electrons as a function of time.

also by the NMR result[16]. The calculated value of σ_e are however about a factor 5 smaller than the experimental ones [2,44]. One might probably ascribe this discrepancy to the crudeness of our electron-ion pseudopotentials, and to the smallness of our molecular dynamics cell which hampers dissociation and recombination processes.

Chapter 6

Summary and Conclusions

In this thesis we have studied the electronic states and dynamical properties of dilute Na-NaBr solutions by using a recently developed Quantum Molecular Dynamics method.

The static structure of electron states in Na-NaBr has been characterized by the radial electron-ion pair correlation functions. Comparing with KCl, we have found that the electron states in NaBr are much more localized and atomic-like than in KCl. The average coordination number is between 2 and 3 in NaBr, whereas the corresponding number for F-center-like states in KCl is about 4. By studying the typical time evolution of the distance between the center of mass of the electron and the ions closest to it, we observed that usually there is a single Na^+ ion which is much closer to the electron than all the others. This means that the configurations in NaBr are typically atomic-like. However Na_2^+-molecular-like and F-center-like configurations are also observed. We have also studied a system with two antiparallel spin electrons. The electron-ion pair correlation function is substantially identical to that

for the single electron case. Furthermore the two electrons attract each other to form a non magnetic complex. The two electron complex is most frequently close to a single Na^+ to form a Na^- species, although other species such as Na_2 molecules and bipolaron-like complexes are also observed. Dissociation of the spin-paired species occur via jumps of one of the electrons. After such jump the two electrons localize in separate spatial positions forming states similar to those of the single electron case.

The jumps are the essential mechanism that determines the electronic conductivity σ_e in our system. The sublinear increase of σ_e with the electronic concentration can be related to the fact that the mobility of the spin-paired species is very low, of the order of the ionic mobility.

Our calculation for the optical absorption spectrum is in very good agreement with the experiment. The experimental observation that the lineshape results from the superposition of two bands can tentatively be related to the existence of dipolar-like states, where the p-like excited states are split into a singlet and a doublet.

In conclusion, we have seen that the structure of the electronic states in dilute metal-metal halide solutions in not uniquely F-center-like, but rather depends on the strength of the potential of the alkali metal atom. In the cases where this potential is sufficiently strong, e.g. in Na-solutions, but most probably also in Li-LiX solutions for which very little experimental information is available, atomic-like states with some dipolar character appear to be favored with respect to the F-center. A dipolar Li atom characteristic of the excitonic state appears to have been observed in the path integral quantun Monte Carlo calculations

of Sprik *et al.*[45], for a single Li atom dissolved in liquid ammonia at $T = 265K$.

The results presented in this thesis are in agreement with earlier speculations and theoretically interpret the anomalous behavior of Na-NaX solutions.

Appendix A

Solution Method for the Time-dependent Schrödinger Equation

We shall be concerned in this appendix with solutions to the time-dependent Schrödinger equation(TDSE) in three Cartesian coordinates, which in atomic units is:

$$i\frac{\partial\psi(x,y,z,t)}{\partial t} = -\frac{1}{2}\nabla^2\psi(x,y,z,t) + V(x,y,z)\psi(x,y,z,t). \qquad \text{(A.1)}$$

where

$$\nabla^2 = \frac{\partial^2}{\partial x^2} + \frac{\partial^2}{\partial y^2} + \frac{\partial^2}{\partial z^2}. \qquad \text{(A.2)}$$

We review briefly the symmetrically split operator algorithm for advancing the solution to Eq.(A.1) by an incremental time Δt. This can be expressed formally as

$$\psi(r, t_0 + \Delta t) = e^{-iH(t)\Delta t}\psi(t)$$

$$= e^{-i\Delta t\nabla^2/4} e^{-i\Delta tV} e^{-i\Delta t\nabla^2/4} \psi(r, t_0) + O[(\Delta t)^3] \qquad \text{(A.3)}$$

Alternatively,

$$\psi(r, t_0 + \Delta t) = e^{-i\Delta tV/2} e^{-i\Delta t\nabla^2/2} e^{-i\Delta tV/2} \psi(r, t_0) + O[(\Delta t)^3] \ . \qquad \text{(A.4)}$$

In Eqs.(A.3) and (A.4), commutation errors give rise to the third order term in Δt, and the operator

$$exp(i\Delta t\nabla^2/4) \qquad \text{(A.5)}$$

applied to $\psi(r, t_0)$ is equivalent to solving the free particle wave equation

$$i\frac{\partial \psi}{\partial t} = -\frac{1}{2}(\frac{\partial^2}{\partial x^2} + \frac{\partial^2}{\partial y^2} + \frac{\partial^2}{\partial z^2})\psi \qquad \text{(A.6)}$$

over a time $\Delta t/2$, with $\psi(x, y, z, t_0)$ as the initial wavefunction at $t = t_0$. The solution to Eq.(A.6) is obtained with help of the band-limited Fourier series representation

$$\psi(x, y, z, t) = \sum_{l=-N/2+1}^{N/2} \sum_{m=-N/2+1}^{N/2} \sum_{n=-N/2+1}^{N/2} \psi_{lmn}(t) exp[\frac{2\pi i}{L_0}(lx + my + nz)], \qquad \text{(A.7)}$$

where

$$\psi_{lmn}(t_0 + \Delta t) = \psi_{lmn}(t_0) exp[-(i\Delta t/2)(2\pi/L_0)^2(l^2 + m^2 + n^2)], \qquad \text{(A.8)}$$

and L_0 is the length of a side of the computational box. The right-hand side of expression (A.3) is thus equivalent to free particle propagation over a half time increment, a phase change from the action of the potential applied over the whole time increment, and an additional free particle propagation over a half time increment. If many factors of the form (A.3) are applied in sequence, pairs of half-step free particle propagation combine into full-step propagations, applied in momentum space,

alternating with phase changes of the wave function executed in configuration space. The only exceptions to this rule are the half steps of propagation applied at the beginning and end of the calculation. This procedure is very efficient and accurate, when implemented with the help of the Fast Fourier Transform (FFT) algorithm.

Appendix B

Conjugate Gradient Minimization of the Energy Functional

Let us suppose that the function f to be minimized can be approximated by a multidimensional quadratic form around some point P taken as the origin of the coordinates

$$f(X) \approx c - < b|X > + < X|A|X > \ , \tag{B.1}$$

where

$$X \equiv (x_1, x_2, ..., x_L) \ , \ c \equiv f(P) \ , \ b \equiv -\nabla f|_P \ , \ A_{ij} \equiv \frac{\partial^2 f}{\partial x_i \partial x_j}|_P \tag{B.2}$$

with a symmetric positive definite $L \times L$ Hessian matrix A. An iterative minimization procedure is then defined by the sequence:

$$P^{(n+1)} = P^{(n)} + \lambda^{(n)} h^{(n)} \quad , \quad n = 0, 1, 2... \tag{B.3}$$

where $\lambda^{(n)}$ is a scalar and $h^{(n)}$ is a vector in multidimensional space. By using the information contained in the matrix of second derivatives A, a

single operation is sufficient to minimize a perfectly quadratic function f. For large L it is impractical to deal with the large matrix A. In the conjugate gradient (CG) method [46] information on A is only used implicitly to define an optimal set of directions $h^{(n)}$ in the sequence of equations (B.3), where the scalar $\lambda^{(n)}$ is obtained by a one-dimensional minimization along the line defined by $h^{(n)}$. The directions $h^{(n)}$ are given by

$$h^{(n)} = \begin{cases} g^{(n)}, & n = 0 \\ g^{(n)} + \gamma^{(n-1)} h^{(n-1)}, & n = 1, 2, 3... \end{cases} \tag{B.4}$$

where

$$\begin{aligned} g^{(n)} &= -\nabla f(P^{(n)}) \\ \gamma^{(n)} &= \frac{< g^{(n+1)} | g^{(n+1)} >}{< g^{(n)} | g^{(n)} >}. \end{aligned} \tag{B.5}$$

The directions $h^{(n)}$ are said to be conjugate. One can show [46] that for a quadratic function like the one in equation (B.1), the following conjugacy property is satisfied

$$< h^{(n)} |\ A\ | h^{(m)} >= 0 \quad \forall n \neq m. \tag{B.6}$$

This property guarantees that each step is actually an improvement over all the preceding ones, a property not shared by steepest descent (SD) based methods. The reason is that SD steps are often orthogonal or nearly orthogonal to one another.

It is natural to apply the CG procedure (equations B.3-5) to the electronic minimization problem. A difficulty arises in this respect because of the existence of orthonormality constraints in the electronic problem. These originate forces of constraint that must be taken into account

when the line minimizations are done. In order to deal with such constraints it is convenient to reformulate the electronic problem in terms of linearly independent but not orthonormal orbitals $\{\varphi_{i\alpha}\}$ (here α is spin label) [40]. The orthonormal orbitals $\{\psi_{i\alpha}\}$ may be related to the $\{\varphi_{i\alpha}\}$ via

$$\psi_{i\alpha} = \sum_j S_{ij,\alpha}^{-\frac{1}{2}} \varphi_{j\alpha} \quad , \tag{B.7}$$

where $S_{ij,\alpha} = < \varphi_{j\alpha} | \varphi_{i\alpha} >$ is the overlap matrix. The energy functional E can be written in terms of the $\{\varphi_{i\alpha}\}$ as

$$E = \sum_{ij,\alpha}^{occ} S_{ij}^{-1} < \varphi_{i\alpha} | -\nabla^2 | \varphi_{j\alpha} > + \int \mathrm{d}\vec{r}\; V^{ext}(\vec{r})\; n(\vec{r}) +$$
$$\int \mathrm{d}\vec{r} \mathrm{d}\vec{r}\,' \frac{n(\vec{r})\; n(\vec{r}\,')}{|\vec{r} - \vec{r}\,'|} + E_{xc}^{LSD}[n\uparrow, n\downarrow] + \sum_{I \neq J} \frac{Z_I Z_J}{|\vec{R}_I - \vec{R}_J|}. \tag{B.8}$$

For initially orthonormal orbitals $\{\varphi_{i\alpha}\}$, one obtains the constrained electronic forces

$$\frac{\delta E}{\delta \varphi_{i\alpha}^*(\vec{r})} = H\varphi_{i\alpha}(\vec{r}) - \sum_m < \varphi_{m\alpha} | H | \varphi_{i\alpha} > \varphi_{m\alpha}(\vec{r}). \tag{B.9}$$

It is convenient to reorthonormalize the $\{\varphi_{i\alpha}\}$ at any step. This will ensure that the S matrix remains nonsingular and allows the use of equation (B.9). Equation (B.9) defines the gradient $g^{(n)}$ from which one obtains the conjugate direction $h^{(n)}$ using equation (B.4). A one-dimensional minimization of the functional E along $h^{(n)}$ allows to compute $\lambda^{(n)}$ and to accomplish the CG step defined in equation (B.3). One possible way to carry out the one-dimensional minimization is to proceed as in nonself-consistent calculation and instead of E minimize $\tilde{E}$ given by [40]

$$\tilde{E}(\lambda^{(n)}) = \sum_{ij,\alpha} < \varphi_{i\alpha}^{(n+1)} | \tilde{H} | \varphi_{j\alpha}^{(n+1)} > S_{ij,\alpha}^{-1\,(n+1)} \quad , \tag{B.10}$$

where $\varphi_{i\alpha}^{(n+1)} = \varphi_{i\alpha}^{(n)} + \lambda^{(n)} h_{i\alpha}^{(n)}$ and $\tilde{H} = \tilde{H}[\{\varphi_{i\alpha}^{(n)}\}]$; i.e. V^H and μ^{xc} are not varied as $\lambda^{(n)}$ is changed but are instead determined by the density corresponding to $\{\varphi_{i\alpha}^{(n)}\}$. In our case of two antiparallel spin electrons, the two wavefunctions must not obey any orthogonalization constraint, but only need to be normalized. In this case the S matrix is simply the norm of the wavefunctions with respect to spin up and down.

Appendix C

Dipolar Atomic States

Logan [21,23] proposed the occurrence of dipolar atomic states in alkali metal-doped matrix systems, based on continuum dielectric theory.

Neither the ns ground state of normal alkali atom nor the np excited states possess any dipolar character, i.e., $< s|\hat{\mu}|s >= 0 =< p_\alpha|\hat{\mu}|p_\alpha >$, where $\hat{\mu}$ is the dipole moment operator. In contrast, matrix elements of $\hat{\mu}$ between s and p states are nonzero: $< s|\hat{\mu_\alpha}|p_\alpha >= M \neq 0$. If, therefore, the alkali atom could hybridize its electrons to produce a state which is a superposition of the s and p states

$$|\Psi(\lambda) >= \frac{|s + \lambda p_z >}{\sqrt{1+\lambda^2}} \tag{C.1}$$

the resultant sp-hybrid state would have a dipole moment

$$< \mu >=< \Psi(\lambda)|\hat{\mu}|\Psi(\lambda) > \tag{C.2}$$

$$= \frac{2\lambda M}{1+\lambda^2} = 2M\sqrt{f_p(1-f_p)}. \tag{C.3}$$

where f_p is the fraction of p_z in the ground state wavefunction, i.e.,

$$f_p = \frac{\lambda^2}{1+\lambda^2}, \tag{C.4}$$

But this involves an energy cost: The hybridization free energy relative to the $\lambda = 0$ nonpolar state is given approximately by

$$E_h(\lambda) = < \Psi(\lambda)|H_0|\Psi(\lambda) > - < \Psi(0)|H_0|\Psi(0) > \quad \text{(C.5)}$$

$$= E_0 \frac{\lambda^2}{1+\lambda^2} \equiv E_0 f_p \qquad \geq 0; \quad \text{(C.6)}$$

where H_0 is the Hamitonian for free alkali atom, E_0 is the $ns - np$ energy difference. In addition, however, the atomic dipole would polarize its surroundings, and would subsequently interact with and be stabilized by the electric reaction field arising due to the polarization induced in the solvent by itself. The stabilization free energy $E_s(\lambda)$ is given by

$$E_s(\lambda) = -\frac{1}{2}\, g(\rho) < \mu >^2, \quad \text{(C.7)}$$

$$= -2g(\rho)M^2 \frac{\lambda^2}{(1+\lambda^2)^2} \leq 0. \quad \text{(C.8)}$$

where $g = (8\pi/3)\rho(\epsilon - 1)/(2\epsilon + 1)$ is the reaction field factor for an insulating matrix, ρ the solvent density, and $\epsilon = \epsilon(\rho, T)$ the solvent dielectric constant[47].

The total free energy $E(\lambda) = E_h(\lambda) + E_s(\lambda)$, given by

$$E(\lambda) = \frac{\lambda^2}{1+\lambda^2}\left\{E_0 - \frac{2g(\rho)M^2}{1+\lambda^2}\right\} \quad \text{(C.9)}$$

$$= \frac{E_0\lambda^2}{1+\lambda^2}\left\{1 - \frac{\alpha_0 g(\rho)}{1+\lambda^2}\right\} \quad \text{(C.10)}$$

is the free energy change of the system consequent upon production of the dipolar atomic state, and relative to the normal ground state with $\lambda = 0$. $\alpha_0 = 2M^2/E_0$ is also defined.

$E(\lambda)$ may be minimized with respect to λ. The minima $E(\lambda)$ occur

at $\lambda_{min} = 0$ and at

$$\lambda_{min}^2 = \frac{\alpha_0 g - 1}{\alpha_0 g + 1}, \quad if \quad \alpha_0 g > 1 \tag{C.11}$$

which correspond to the normal and dipolar atomic states respectively. Thus, the total free energy E may be expressed in terms of λ

$$E(\lambda) = \frac{E_0 \lambda^2}{1+\lambda^2}\left\{1 - \frac{1}{1-\lambda^2}\right\} \tag{C.12}$$

$$= -\frac{E_0 \lambda^4}{(1+\lambda^2)(1-\lambda^2)} \tag{C.13}$$

We can also express E in terms of f_p

$$E(f_p) = -E_0 \frac{f_p^2}{1-2f_p}. \tag{C.14}$$

Now let us consider the excitation spectrum of the dipolar atom. The model Hamitonian H_0 for the isolated alkali atom is taken by Logan as a simple quantum mechanical four-level system (FLS), which only includes a single ns orbital with energy $\epsilon_0 = -\hbar\omega_0$ and three np orbitals lying at energy $\epsilon_1 = \hbar\omega_0$, where the zero in energy is arbitrarily taken as midway between the $ns-$ and $np-$ orbital energies. Higher excited states of the atom are neglected due to the fact that the lowest excited n^2P term being well separated in energy from higher excited states.

The electric reaction field arising due to the dielectric response of the alkali metal-doped matrix, induced by the dipolar alkali atom itself, introduces a perturbation V to H_0. With the chosen basis, the four eigenvalues obtained by diagonalizing the Hamitonian $H = H_0 + V$ are, $\hbar\omega_-^0$, $\hbar\omega^0$ (double degenerate), and $\hbar\omega_+^0$, where ω_-^0 and ω_+^0 are given by

$$\omega_\pm^0 = \pm[\omega_0^2 + (gM < \mu >_0 /\hbar)^2]^{1/2} \tag{C.15}$$

We now relable the np wavefunctions in $|P_m>$ notation ($m = 0, \pm$), where $m\hbar$ gives the component of the electronic orbital angular momentum about the axis specified by the direction of the induced atomic dipole moment. The normalized, orthogonal eigenfunction corresponding to ω_-^0, ω_0, and ω_+^0 are denoted by $|\Psi_-^0>, |\Psi_0^0>$, and $|\Psi_+^0>$, respectively, and are given by

$$|\Psi_-^0> = \frac{|s + \lambda p_0>}{\sqrt{1+\lambda^2}} \tag{C.16}$$

$$|\Psi_0^0> = |p_1> and |p_{-1}> \tag{C.17}$$

$$|\Psi_+^0> = \frac{|p_0 - \lambda s>}{\sqrt{1+\lambda^2}} . \tag{C.18}$$

In Fig. C.1 a summary in terms of the eigenvalues and eigenfunctions are presented for the normal state and for the dipolar atomic state. For convenience when discussing the optical spectra, the splitting Δ_{EI} is defined such as

$$\omega_\pm(0) = \pm(\omega_0 + \Delta_{EI}) \tag{C.19}$$

where

$$\Delta_{EI} = \omega_0 \left(\left\{ 1 + \frac{\alpha_0}{\hbar\omega} [g < \mu >_0]^2 \right\}^{1/2} - 1 \right) \tag{C.20}$$

By using eqs.(C.4) and (C.11), it can be expressed in terms of f_p and E_0:

$$\Delta_{EI} = E_0 \frac{f_p}{1 - 2f_p}. \tag{C.21}$$

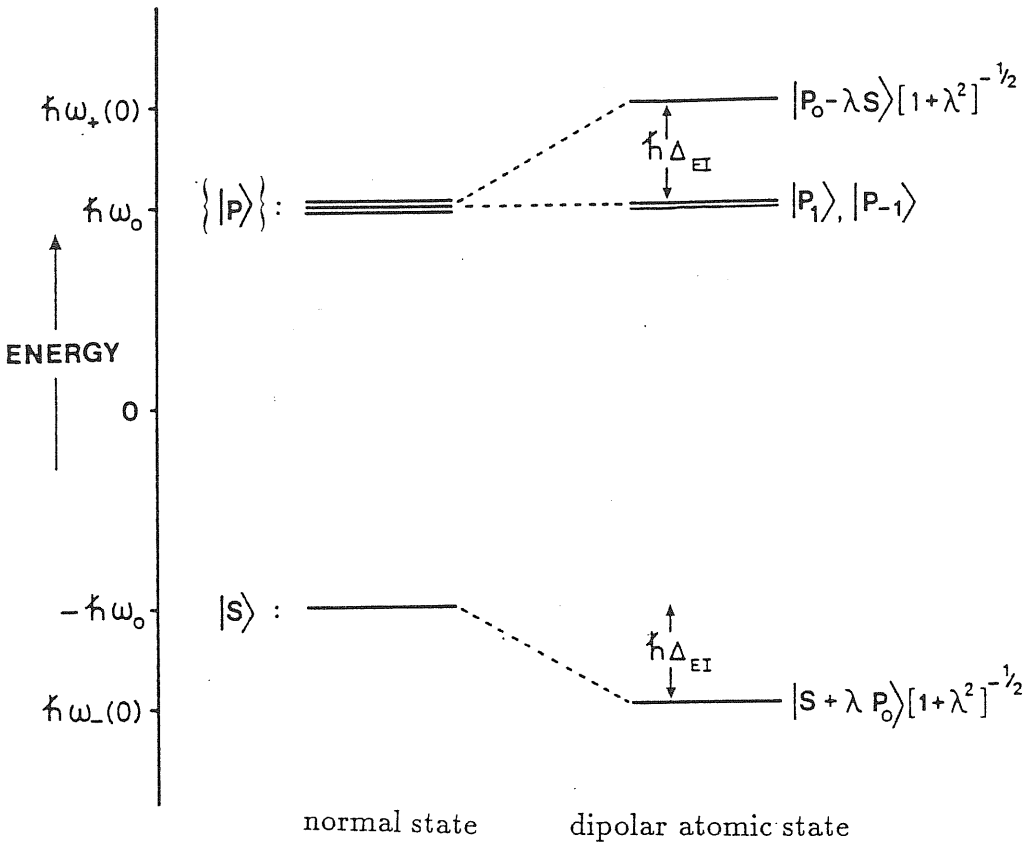

Figure C.1: Summary of the eigenvalues and eigenvectors of the normal state and the dipolar atomic state.

Bibliography

[1] *For a general rewiew, see* : W.W. Warren Jr., in *The Metallic and Non-Metallic States of Matter: An Important Facet of The Chemistry and Physics of The Condensed State.* Edited by P.P. Edwards and C.N.R. Rao (Taylor and Francis, London, 1985).

[2] M.A. Bredig, in *Molten Salt Chemistry* , edited by M. Blander (Interscience, New York, 1964).

[3] W. Freyland, K. Garbade, and E. Pfeiffer, Phys. Rev. Lett. **51**, 1304 (1983).

[4] W. Freyland, K. Garbade, H. Heyer and E. Pfeiffer, J. Phys. Chem. **88**, 3745 (1984);
W. Freyland, private communication.

[5] W. Schmitt and U. Schingewolf, Ber. Bunsenges. Phys. Chem. **81**, 584 (1977).

[6] K.S. Pitzer, J. Am. Chem. Soc., **84**, 2025 (1962)

[7] N. Nicoloso, and W. Freyland, Z. Phys. Chemie **135**, 39 (1983).

[8] W.W. Warren Jr., S. Sotier, and G.F. Brennert, Phys. Rev. **B30**, 65 (1984).

[9] N. Nicoloso, and W. Freyland, J. Phys. Chem. **87**, 1997 (1983).

[10] M. Parrinello, and A. Rahman, J. Chem. Phys. **80**, 860 (1984).

[11] A. Selloni, P. Carnevali, R. Car, and M. Parrinello, Phys. Rev. Lett. **59**, 823 (1987).

[12] H.R. Bronstein and M.A. Bredig, J. Am. Chem. Soc., **80**, 2077 (1958).

[13] I. Katz and S.A. Rice, J. Am. Chem. Soc., **94**, 4824 (1972).

[14] P.J. Durham and D.A. Greenwood, Phil. Mag., **33**, 427 (1976).

[15] W.W. Warren Jr., B.F. Campbell, and G.F. Brennert, Phys. Rev. Lett. **58**, 941 (1987).

[16] W.W. Warren Jr., S. Sotier, and G.F. Brennert, Phys. Rev. Lett. **50**, 1505 (1983).

[17] P. Littlewood, Phys. Rev. **B24**, 1710 (1981).

[18] J. J. Markham, *F-centers in Alkali Halides*, Solid State Physics, Suppl. 8, (Academic Press, New York, 1966).

[19] W. B. Flowler, in *Physics of Colour Centers*, edited by W.B. Flowler, (Academic Press, New York, 1968).

[20] E.S. Fois, A. Selloni, M. Parrinello, and R. Car, J. Phys. Chem. **92**, 3268 (1988).

[21] D.E. Logan, Phys. Rev. Lett. **57**, 782 (1986).

[22] D.E. Logan and P.P. Edwards, Ber. Bunsenges. Phys. Chem. **90**, 575 (1986).

[23] D.E. Logan, J. Chem. Phys. **86**, 234 (1987).

[24] M. Parrinello, and A. Rahman, to be published.

[25] R. Car, and M. Parrinello, Phys. Rev. Lett. **55**, 2471 (1985).

[26] *see, for instance*: D. W. Heermann, Computer Simulation Methods In Theoretical Physics (Springer, Berlin, 1986) and Wm. G. Hoover, Molecular Dynamics (Springer, Berlin, 1986).

[27] *see, for instance*: J. C. Tully, in *Dynamics of Molecular Collisions, part B*, edited by W. H. Miller, (Plenum Press, New York, 1976), and references therein.

[28] L. Verlet, Phys. Rev. **159**, 98 (1967).

[29] J.A. Fleck, J.R. Morris, and M.D. Feit, Appl. Phys. **10**, 129 (1976).

[30] M.D. Feit, J.A. Fleck and A. Steiger, J. Comp. Phys. **47**, 412 (1982).

[31] *See, for instance : Theory of Inhomogeneus Electron Gas* edited by S. Lundqvist, and N.H. March, (Plenum, New York 1983) and references therein.

[32] O. Gunnarson, B.I. Lundqvist, Phys. Rev. **B13**, 4274 (1976).

[33] D. M. Ceperley and B. J. Alder, Phys. Rev. Lett. **45**, 566 (1980).

[34] J. P. Perdew and A. Zunger, Phys. Rev. **B23**, 5048 (1981).

[35] D.J. Adams and I.R. McDonald, J. Phys. C: Solid State Phys. **7**, 2761 (1974).

[36] F.G. Fumi and M.P. Tosi, J. Phys. Chem. Solids **25**, 31 (1964).

[37] R.W. Shaw, Phys. Rev. **174**,769 (1968).

[38] G.B. Bachelet and M. Schluter, Phys. Rev. **B25**, 2103 (1982).

[39] R. Car, M. Parrinello and W. Andreoni, in *Microcluster*, edited by S. Sugano, Y. Nishina and S. Ohnishi, Springer Series in Material Science **4**, 134 (1987).

[40] I. Štich, R. Car, M. Parrinello and S. Baroni, Phys. Rev. **B39** 4997 (1989).

[41] R.J. Bell and P. Dean, Disc. Faraday Soc. **50**, 55 (1970).

[42] E.S. Fois, A. Selloni and M. Parrinello, Phys. Rev. **B39**, 4812 (1989).

[43] *See, for instance :* E.N. Economou, Green's Functions in Quantum Physics, Springer Series in Solid State Science, Vol.7; (Springer, Berlin, 1983), p152.

[44] G.M. Haarberg, K.S. Osen, J.J. Egan, H. Heyer and W. Freyland, to be published.

[45] M. Sprik, M.W. Impey and M.L. Klein, Phys. Rev. Lett. **56**, 2326 (1986).

[46] W.M. Press, B.P. Flannery, S.A. Teukolsky, and W.T. Vetterling, *Numerical Recipes*, (Cambridge University, Cambridge, 1986).

[47] H. Fröhlich, *Theory of Dielectrics*, (Oxford University, Oxford, 1958).